

---

Masters Theses

Student Theses and Dissertations


---

1972

## Calculation of buildup factors for multilayer slab shields using the Monte Carlo method

John Paul Kuspa

Follow this and additional works at: [https://scholarsmine.mst.edu/masters\\_theses](https://scholarsmine.mst.edu/masters_theses)

 Part of the [Nuclear Engineering Commons](#)

Department:

---

### Recommended Citation

Kuspa, John Paul, "Calculation of buildup factors for multilayer slab shields using the Monte Carlo method" (1972). *Masters Theses*. 5114.  
[https://scholarsmine.mst.edu/masters\\_theses/5114](https://scholarsmine.mst.edu/masters_theses/5114)

This thesis is brought to you by Scholars' Mine, a service of the Curtis Laws Wilson Library at Missouri University of Science and Technology. This work is protected by U. S. Copyright Law. Unauthorized use including reproduction for redistribution requires the permission of the copyright holder. For more information, please contact [scholarsmine@mst.edu](mailto:scholarsmine@mst.edu).

CALCULATION OF BUILDUP FACTORS FOR  
MULTI-LAYER SLAB SHIELDS USING THE  
MONTE CARLO METHOD

BY

JOHN PAUL KUSPA, 1946-

A THESIS

Presented to the Faculty of the Graduate School of the

UNIVERSITY OF MISSOURI-ROLLA

In Partial Fulfillment of the Requirements for the Degree

MASTER OF SCIENCE IN NUCLEAR ENGINEERING

1972

Approved by

*N. Tsoulfanidis* (Advisor)

*D. Ray Edwards*

*John L. Best*

## ABSTRACT

Gamma-ray beams normally incident upon slab shields of varying compositions are studied using a computer program based upon the Monte Carlo technique. Initial gamma energies of 1, 4, 6, and 8 MeV are considered. The shielding materials used were aluminum, iron, and lead. Both single and double material shields were investigated, at a variety of thicknesses up to a maximum of five mean free paths. Two secondary gamma processes are included in this simulation: annihilation gammas from pair production and bremsstrahlung from the electrons. The primary effort is the calculation of the dose, energy, and number buildup factors for these shields. The results for a single material agree quite well with experimental values, and the double material results agree with previous calculations. Secondary results obtained include the pattern of energy deposition within the shield and the variation in beam energy and radial spectra as it passes through the shield. The most important conclusion resulting from this work is that secondary gammas must be considered to obtain valid results when studying heavy materials at incident gamma energies greater than 1 MeV.

## ACKNOWLEDGEMENT

This work would not have been possible without the effective guidance of my advisor, Dr. Nick Tsoulfanidis. His insight into the theory of the physical processes involved enabled a successful computer simulation to be developed. Equally important was his previous experience in applying the principles of the Monte Carlo technique to the most subtle points of the simulation. His continuous advice and encouragement are deeply appreciated.

Several other faculty and graduate student members of the Nuclear Engineering Department were of great assistance. Dr. D. R. Edwards participated in helpful discussions. Graduate students Charles Kalter, Glenn Schade, Charles Gill, and Dan Smith assisted in the details of the computer program. Mr. Kalter was most helpful in providing advice on the Monte Carlo aspects of the program throughout the course of this work.

## TABLE OF CONTENTS

	Page
ABSTRACT.....	ii
ACKNOWLEDGEMENT.....	iii
TABLE OF CONTENTS.....	iv
LIST OF ILLUSTRATIONS.....	vii
LIST OF TABLES.....	viii
I. INTRODUCTION.....	1
A. DESCRIPTION OF THE PROBLEM.....	1
B. REVIEW OF THE LITERATURE.....	3
C. NEED FOR THE PRESENT WORK.....	3
II. DEVELOPMENT OF THE MONTE CARLO PROGRAM.....	5
A. PRINCIPLES INVOLVED.....	5
B. TYPES OF PARTICLE INTERACTIONS.....	5
1. PHOTOELECTRIC EFFECT.....	5
2. COMPTON SCATTERING.....	7
3. PAIR PRODUCTION.....	8
C. GAMMA-RAY TRACKING.....	9
1. GENERAL APPROACH.....	9
2. DETERMINATION OF THE DISTANCE BETWEEN TWO SUCCESSIVE INTERACTIONS AND THE LOCATION OF EACH INTERACTION.....	11
3. SELECTION OF THE TYPE OF INTERACTION.....	12
4. DIRECTION AND ENERGY OF THE PHOTON AFTER COMPTON SCATTERING.....	13
5. GAMMAS RESULTING FROM PAIR PRODUCTION.....	15
6. DETECTING EMERGING PHOTONS.....	17

Table of Contents (continued)	Page
D. ELECTRON AND POSITRON TRACKING.....	18
1. GENERAL CONSIDERATIONS.....	18
2. ELECTRON ENERGY, DIRECTION, AND RANGE.....	19
3. ENERGY DEPOSITION.....	22
4. BREMSSTRAHLUNG.....	24
E. PROGRAM CAPABILITIES.....	27
1. OVERALL CONSIDERATIONS AND INITIALIZATION.....	27
2. PRIMARY RESULTS.....	28
3. SECONDARY RESULTS.....	30
4. ANALYSIS OF THE RUN.....	31
5. CHECKS PERFORMED IN THE DEVELOPMENT OF THE PROGRAM.....	33
III. RESULTS AND CONCLUSIONS.....	37
A. BUILDUP FACTORS.....	37
1. CASES CONSIDERED.....	37
2. SINGLE MATERIAL SHIELDS.....	38
3. DOUBLE MATERIAL SHIELDS.....	41
B. SECONDARY RESULTS.....	47
1. ENERGY DEPOSITION.....	47
2. ENERGY AND SPATIAL DISTRIBUTIONS OF GAMMAS AT INTERFACES.....	49
C. CONCLUSIONS.....	52
D. RECOMMENDATIONS FOR FURTHER WORK.....	53
BIBLIOGRAPHY.....	56
VITA.....	58

Table of Contents (continued)	Page
APPENDICES.....	59
A. BLOCK DIAGRAM FOR THE COMPUTER PROGRAM.....	59
B. DATA USED.....	60
C. DETERMINATION OF THE POSITION OF EACH INTERACTION.....	64
D. COORDINATE SYSTEM TRANSFORMATIONS.....	66
E. TRACKING THROUGH MATERIAL INTERFACES.....	73
F. ENERGY DEPOSITION ZONES.....	76
G. ERROR ANALYSIS.....	79

## LIST OF ILLUSTRATIONS

Figures	Page
1. Schematic of all the possible interactions which are simulated.....	6
2. Typical Klein-Nishina distribution function for $\theta$ selection.....	13
3. Two beam and detector size combinations considered.....	35
4. Dose buildup factors for single material (iron) shields, as a function of thickness, at gamma energies of 6 and 8 MeV..	39
5. Dose buildup factors for single material (lead) shields, as a function of thickness, at gamma energies of 6 and 8 MeV..	40
6. Energy buildup factors for 4 mfp of a composite shield of aluminum and lead, at gamma energies of 1, 4, and 8 MeV.....	43
7. Number buildup factors for 4 mfp of a composite shield of aluminum and lead, at gamma energies of 1, 4, and 8 MeV.....	44
8. Dose buildup factors for 4 mfp of a composite shield of aluminum and lead, at gamma energies of 1, 4, and 8 MeV.....	45
9. Various energy deposition patterns in lead and aluminum shields at 1 MeV.....	48
10. Interface numbering system used in the energy and radial distributions for gamma-rays.....	50
11. Energy and spatial distributions at each interface of an Al-Pb shield at 1 MeV for 2000 original gamma-rays.....	51
12. a. Gamma tracking as seen from the fixed coordinate system.....	67
b. Local System (Step 0) - Translate origin to the beginning of the first gamma vector.....	67
c. Local System (Step 1) - Rotate about $z_0^1$ through angle $\phi_1$ .....	67
d. Local System (Step 2) - Rotate about $y_1^1$ through angle $\theta_1$ .....	68
e. Local System (Step 3) - Translate to the end of the current vector.....	68
13. Gamma tracking through the interfaces of a double material shield.....	74
14. Electron tracking through the energy deposition zones of a double material shield.....	77



## LIST OF TABLES

Tables	Page
1. Material Properties.....	60
2. Pair production attenuation coefficients, $\mu_{pp}$ (cm <sup>2</sup> /gm).....	62
3. Attenuation coefficients, $\mu$ and $\mu_c$ (cm <sup>2</sup> /gm).....	63

## I. INTRODUCTION

### A. Description of the Problem

Gamma radiation impinging upon a shielding material gives rise to two radiation components within or beyond the shield. At any given penetration depth, one radiation component consists of those particles which have not had an interaction. The number of these noninteracted particles decreases exponentially with penetration distance. The other component consists of those particles which have had one or more interactions and still reached that point, as well as those which were created within the material through secondary processes.

In studying radiation attenuation through a medium, one is interested in particular quantities, such as the number of particles at a certain point, the energy of all those particles reaching that point, or the radiation dose that would be absorbed there by tissue. Regardless of which of these quantities is to be calculated, the total number of particles at any point should be known.

Instead of calculating the total number of particles and their corresponding energies, it is advantageous to determine a ratio, known as a buildup factor, defined as follows:

$$B = \frac{\text{Quantity at a point due to the total number of particles}}{\text{Quantity at a point due only to noninteracted particles}} \quad (1)$$

The quantity calculated might be the number of particles, their energy, or the dose imparted by them, thereby giving rise to number, energy, and dose buildup factors, respectively. Buildup factors depend on the radiation (energy and particle type), the medium being traversed, and

the geometry (parallel beam, isotropic source, slab configuration, infinite medium, etc.). The main advantage of using the concept of a buildup factor is that the ratio expressed by Eq. (1) changes slowly with changes in geometry, radiation, energy, and material. Thus, the study of a small number of cases can provide information for other problems with different parameters.

The purpose of this work is to calculate the buildup factor of gamma-rays in multi-region shields, for various beam energies, slab thicknesses, and shielding arrangements and compositions. As very useful by-products, the change in both the energy and spatial distribution of the gamma beam as it passes through the shield, as well as a measure of the amount of energy that is deposited within the shield as a function of the penetration depth, are also obtained.

One way to perform buildup factor calculations is by using the solution of the Boltzmann transport equation. Solutions to this equation can be obtained for simple cases involving one shielding material, but extension to multi-region shields is extremely difficult to accomplish. The present work uses the Monte Carlo method. The Monte Carlo technique offers the advantages of complete flexibility with respect to beam characteristics, shield dimensions and geometry, combinations of materials, and parameters to be measured and studied. The approach taken is to follow the life histories of many individual particles as they pass through the shield. The transport processes within the shield are developed from the theory. The different changes or events in the life of a particle are decided with the use

of probabilities for individual particle interactions. A computer program that simulates these particle histories and performs the necessary computations has been developed. The results are obtained just as they would be from an experiment, except that the computer performs the needed "measurements".

## B. Review of the Literature

Much of the basic theory is adequately covered in standard textbooks dealing with interaction of gamma-rays with matter [1,2,3, 4,5]. In addition, several books and articles have been published which provide buildup factors either as the result of calculations or physical experiments, or both [6,7,8,9,10].

Many Monte Carlo programs have been developed to study the buildup effect, with the degree of success highly dependent on the assumptions used and the specific cases considered. The main difference between the various programs comes from the way in which secondary gamma-rays (bremsstrahlung and pair production gammas) are treated. For example, for shielding materials of high atomic number ( $Z$ ), such as lead, Johnson [7] shows that a significant disparity with experimental results occurs if bremsstrahlung radiation is neglected.

## C. Need for the Present Work

Several semi-empirical formulae [6:230] have been developed to calculate the buildup factors for multi-region shields, with varying degrees of success. These are generally based on the assumption that the buildup factors for each individual material comprising the shield

are known at all pertinent energies and thicknesses. Also, these buildup factors must correspond to the particular radiation source and shielding geometry for the composite shield being studied. It is therefore typically difficult to apply these equations to a wide range of materials, geometries, and incident gamma-ray energies. Calculation of the buildup factors using Monte Carlo simulation can be a more flexible and often a more accurate approach, particularly when applied to multi-layer shields and when both primary and secondary radiation are considered. This work considers secondary radiation in the study of multi-layer shields, yielding results which agree very well with experiments.

## II. DEVELOPMENT OF THE MONTE CARLO PROGRAM

### A. Principles Involved

In order to follow a gamma particle through a medium properly, one must account for every possible event within the materials comprising the shield. The following quantities are critical: the distance the particle travels in a given direction between two successive interactions, the type of interaction which then occurs, and the new direction and energy the gamma assumes if it emerges from the interaction. Tracking continues for the individual particle until it penetrates the shield or it has been absorbed within it. The energy and direction of all emerging particles is recorded and stored, and these can be used for calculations of dose, energy, or number buildup factors. Decisions concerning the fate of the particle in each step of its history are based upon the possible types of interactions and the products resulting from these interactions.

### B. Types of Particle Interactions

There are three main interactions for a gamma-ray moving in a medium. These are the photoelectric effect, Compton scattering, and pair production. Each of these is discussed in detail, and Fig. 1 provides an overall view of the events which are considered in this simulation.

#### 1. Photoelectric Effect

In this process (see point 4, Fig. 1), the photon interacts with an entire atom to eject an electron from one of its atomic shells



[3:130]. The gamma-ray is absorbed, and its life history is terminated. The probability for the photoelectric effect to occur ( $\mu_{pe}$ ) is related to the gamma-ray energy ( $E_\gamma$ ) and the atomic number ( $Z$ ) of the medium by [1:698]:

$$\mu_{pe} \sim Z^4/E^3 \quad (2)$$

This effect is dominant at low gamma energies, diminishing greatly around 1 MeV for most materials. Since  $\mu_{pe}$  increases rapidly with  $Z$ , this "total absorption" effect is much more pronounced in lead, for example, than in aluminum, a much lighter material, for the same gamma energy.

## 2. Compton Scattering

Here the photon interacts with a free electron [3:132]. This interaction (see points 1 and 5, Fig. 1) is a two-body collision, and standard kinematics of conservation of energy and momentum apply. As a result of Compton scattering, the gamma-ray is deflected, with part of its energy given to the recoil electron. In this case, the life history is continued, but the reduced energy of the gamma and its new direction must be considered in subsequent steps. The Compton effect is considered to be absorptive only in the sense that some of the gamma energy has been removed from the beam and transferred to the electron. The electron reemits some energy as bremsstrahlung and deposits the rest in the shielding material as ionization and excitation energy.



The probability for Compton scattering to occur ( $\mu_c$ ) is roughly independent of  $Z$ ; but it is a complicated, although relatively smooth, function of  $E_\gamma$ . The Compton effect is dominant at energies of about 1 MeV.

### 3. Pair Production

This event (see point 2, Fig. 1), in which the photon disappears and a positron-electron pair is formed, occurs in the presence of a heavy nucleus [3:135]. Since the total rest mass energy of the two particles thus formed is  $2 \times 0.511 \text{ MeV} = 1.022 \text{ MeV}$ , pair production is not possible if the gamma energy is below this threshold energy. The probability for pair-production to occur ( $\mu_{pp}$ ) increases with photon energy and with the atomic number of the material (roughly as  $Z^2$ ) [3:137].

Pair production is a totally absorptive process with respect to the incident gamma. The positron and the electron deposit their energies much as a recoil Compton electron does, partly in ionization and excitation, and partly as bremsstrahlung. When the positron comes to rest and encounters an electron, the two annihilate, and their rest mass appears as two new gammas, each with 0.511 MeV. Since these photons can impart a dose at the detector if they emerge, these annihilation gammas are potentially an important source of "scattered" radiation. Therefore, they can contribute a significant amount to the scattered dose, which is precisely the quantity to be determined in computing the dose buildup factor correctly. Thus, these histories must also be considered.

## C. Gamma-Ray Tracking

### 1. General Approach

Gamma tracking is the main task of the program, and it is subdivided into many routines. To start a history, seven variables are assigned for each particle: three coordinates, three direction cosines, and energy. Then, an internal loop is established to cycle through each interaction in which this particle may be involved. There are many ways in which the particle may leave this scattering loop.

- a. The particle emerges from either the front or back faces of the slab, or exits via the sides of the shield.
- b. The energy falls below a preset minimum, hence further calculations are unwarranted due to the negligible energy remaining.
- c. The gamma-ray is totally absorbed in the photoelectric effect.
- d. The number of scatterings exceeds a preset limit. This prevents an improbable but possible infinite loop from consuming computer time on a particle which, if it does eventually emerge, will not have sufficient energy to have a noticeable effect.

Each of these terminal occurrences are recorded, and a new particle is started through the system. If the particle has emerged from the back face, where the detector is located, a detection routine is used to make the buildup calculations.

If none of these terminal conditions are met, the scattering loop is followed. The first calculation is the determination of the various  $\mu$  values for the current energy of the particle. Linear

interpolation is used when this energy falls between the tabular energies input for the materials. The distance to the next interaction is then calculated from the total attenuation coefficient. Using this distance and the current direction cosines relative to the fixed coordinate system of the shield, the position of the next interaction is found. If this new location is still within the slab, the type of interaction at that point can be determined next. However, if the latest path has intersected an internal region boundary between two shielding materials, then a separate routine is entered to find how much further the particle penetrates the new material, based on the same gamma energy, but with a different set of  $\mu$  values corresponding to the new material.

Once an event location within a material region is identified, the relative probabilities for an interaction outcome are computed. Using a random number, the actual outcome based on these probabilities is found. Only if Compton scattering has occurred does the scattering routine continue without modification. Then, the rejection technique of Monte Carlo [11:26] is employed to find the scattering angle, which also uniquely determines the amount of energy the gamma retains after the interaction. The history then continues with this new energy and direction. If pair production occurs, a special routine is used to track the two annihilation gammas produced. All these routines that track the various gamma-rays are discussed in detail in the sections which follow.

## 2. Determination of the Distance Between Two Successive Interactions and the Location of Each Interaction

The total probability that the photon will interact through any of the three types of possible events is the sum of the three individual probabilities:

$$\mu = \mu_{pe} + \mu_c + \mu_{pp} \quad (3)$$

where  $\mu$  is the total linear attenuation coefficient, in units of  $\text{cm}^{-1}$ . The attenuation coefficient is a function of material and gamma energy. The reciprocal of  $\mu$  is the average distance (cm) that the photon travels between two successive interactions, and this is known as the mean free path. The probability that a photon will travel a distance  $x$  without an interaction is  $e^{-\mu x}$ . The exponential nature of the gamma-ray attenuation can then readily be expressed as:

$$N(x) = N_0 e^{-\mu x} \quad (4)$$

where  $N(x)$  is the number of unscattered gamma-rays at penetration distance  $x$ , and  $N_0 = N(0)$ , the original number of incident gammas.

The basic idea of Monte Carlo simulation is to select distances  $x$  such that if the selection process is repeated indefinitely, these distances will be distributed as  $e^{-\mu x}$ . This is achieved if one sets:

$$r = e^{-\mu x} \quad (5)$$

where  $r$  ( $0 \leq r \leq 1$ ) is a random number. Then, solving for  $x$ :

$$x = -\ln(r)/\mu \quad (6)$$

the distances ( $x$ ) selected in this manner are distributed exponentially, and their average is  $\mu^{-1}$ , or one mean free path.

The distance selected randomly in this fashion is then used to find the location of the next event by updating the gamma coordinates. The basic approach is to keep track of the latest gamma vector's direction in terms of direction cosines. Then, each of the coordinate increments is found by multiplying the distance selected by the appropriate direction cosine. To be able to keep track of these successive positions and vectors in the fixed coordinate system, a geometric transformation is used after each event. This is described in detail in Appendices C and D.

### 3. Selection of the Type of Interaction

The type of interaction at any position is determined by using a random number and the relative probabilities for the three main types of interaction to occur. These probabilities are:

$$\mu_{pe}/\mu = \text{Relative probability that photoelectric effect will occur} \quad (7a)$$

$$\mu_c/\mu = \text{Relative probability that Compton scattering will occur} \quad (7b)$$

$$\mu_{pp}/\mu = \text{Relative probability that pair production will occur} \quad (7c)$$

A random number ( $r$ ) is selected, and if  $r \leq \mu_{pe}/\mu$ , then the photoelectric effect has occurred. If  $\mu_{pe}/\mu < r \leq (\mu_{pe} + \mu_c)/\mu$ , then Compton scattering has taken place. Otherwise,  $r > (\mu_{pe} + \mu_c)/\mu$ , and pair production has occurred.

This event determination is made once the interaction position has been found. Since  $\mu$  and each of its components is a function of the gamma-ray energy and the shielding material, these attenuation

coefficients are calculated for each interaction or each time a new material region is entered by the gamma being tracked.

#### 4. Direction and Energy of the Photon after Compton Scattering

Compton scattering is not isotropic. The probability that the photon will have a collision and scatter to an angle  $\theta$  is given by the differential Compton scattering cross section, known as the Klein-Nishina formula [1:683]:

$$\frac{d\sigma}{d\Omega} = \frac{r_0^2}{2} \left(\frac{\nu'}{\nu_0}\right)^2 \left[\frac{\nu_0}{\nu'} + \frac{\nu'}{\nu_0} - \sin^2\theta\right] \quad (8)$$

where  $\nu_0$  and  $\nu'$  are the frequencies of the incident and emerging gamma-rays, respectively. As the photon energy increases, Compton scattering becomes strongly forward peaked. Again, using random numbers, the angle of scattering,  $\theta$ , is selected in such a way that after many  $\theta$ 's are selected, their distribution is that given by the Klein-Nishina formula.

A method known as the rejection technique [12:10] is used for  $\theta$  selection. Consider a typical plot of the distribution function

$$f(\theta) = (d\sigma/d\Omega) / (d\sigma/d\Omega)_{\max} \quad (9)$$

shown in Fig. 2 below.

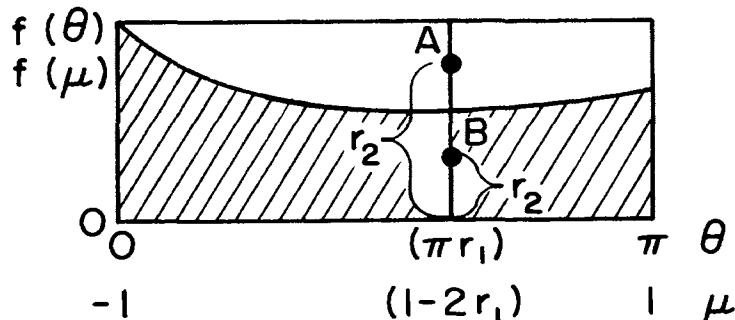


Figure 2: Typical Klein-Nishina distribution function for  $\theta$  selection

A pair of random numbers  $(r_1, r_2)$  is selected. If the point (A) with coordinates  $(\pi r_1, r_2)$  falls outside the shaded area of Fig. 2, the random pair is rejected, and a new pair is selected. Once a coordinate pair (B) thus selected falls within the shaded region, that pair is accepted, and the scattering angle for that interaction is:

$$\theta = \pi r_1 \quad (10)$$

In the program it is more convenient to change variables from  $\theta$  to  $\mu = \cos\theta$ , where  $(-1 \leq \mu \leq +1)$ , and  $\mu$  is not to be confused with the attenuation coefficient. Once an acceptable pair of random numbers, based on the coordinates  $(1-2r_1; r_2)$ , has been found, the scattering angle is found directly from its cosine:

$$\theta = \arccos(\mu) = \arccos(1-2r_1) \quad (11)$$

The efficiency of the rejection technique is simply the ratio of the shaded area of Fig. 2 to the total area shown, if the coordinate pairs are selected to be uniformly distributed over the total area. However, by selecting the coordinate pairs for a particular distribution in a special manner, it is possible to improve the efficiency of the rejection scheme [13]. Kahn [12:62] has developed a more efficient selection scheme for the Klein-Nishina distribution function, and this is the method used in the program.

The other angle of scattering,  $\phi$ , is completely random and can be found from the simple expression:

$$\phi = 2\pi r \quad (12)$$

where  $r$  is another random number.

Since Compton scattering is a two particle collision, conservation of energy and momentum requires that, if a photon of energy  $E_\gamma$  is scattered to an angle  $\theta$ , its energy after the collision is  $E'_\gamma$ , which is found by [1:675]:

$$E'_\gamma (\text{MeV}) = \frac{E_\gamma (\text{MeV})}{1 + (E_\gamma / .511)(1 - \cos\theta)} \quad (13)$$

Hence, for each scattering, the new direction and energy can be determined for the emerging gamma, and the tracking for this history can continue. Appendices C and D give the details on how the coordinates for each successive interaction are found.

#### 5. Gammas Resulting from Pair Production

Thusfar, only the tracking of gammas undergoing Compton scattering has been discussed. If the photoelectric effect occurs, the process is totally absorptive, that outcome is tallied, and a new history is begun. The third possible outcome is the formation of a positron and an electron in pair production, with the disappearance of the incident gamma at that point. This process is totally absorptive as far as the original gamma is concerned. Hence, this could be handled just as in the photoelectric case. However, when the positron comes to rest and is annihilated upon meeting an electron, two fresh gammas are produced, each with energy equal to the electron rest mass, 0.511 MeV. Since pair production can occur only when the incident gamma has energy greater than 1.022 MeV, these fresh gammas need not be accounted for if the program is to be used for 1 MeV cases or below. This work, can handle energies above 1 MeV, therefore, these



extra pair production gammas are accounted for in the calculation of the buildup factor.

Since the bulk of the program is already geared to handle gamma tracking, maximum use is made of existing routines in simulating the effect of these annihilation gammas. The simplest way to accomplish this is to treat the first of these two gammas as a continuation of the incident gamma which was actually absorbed in the pair production event. The positron might travel up to a couple of centimeters before annihilation, but a good initial approximation is to assume that these new gammas are emitted at the same point where the pair production occurred, thereby eliminating the need to track the positron and perform a new coordinate transformation to obtain the true birth point of these gammas. Then the process can be treated just as in Compton scattering. However, here the "scattering" angle is selected isotropically ( $\theta = \pi r$ ), and the new gamma energy is defined to be 0.511 MeV, not a function of  $\theta$  as it would be in a true scattering. The tracking can now continue as if the first new particle were the original gamma. This particle will not have sufficient energy to later be involved in a new pair production event, hence a cascade effect is not possible. The history can be continued until it is ultimately absorbed or it emerges from the shield.

Once this combined history is concluded, the program would normally try to select the next incident particle for study. However, a special provision is made so that the second annihilation gamma is tracked first. The material region and birth coordinates of the two

gammas are saved as soon as the pair production interaction occurs. Also needed are the direction cosines at birth. Since these two gammas are emitted back to back, the direction cosines of the first gamma are saved. Then, to get the opposing vector for the second gamma, the sign on each of the three original direction cosines at birth are reversed. Since the second annihilation gamma will be initiated just as an incident particle would be, the transformation matrix (see Appendix D) is reset appropriately.

A special count is kept of the number of pair production gammas which are actually detected. For high incident gamma energies and high Z materials, where production is most significant, these annihilation gammas often comprise up to 25% of the scattered radiation observed by the detector. This routine, therefore, greatly enhances the accuracy of the buildup factor calculations. Fig. 1 depicts each of the possible interactions which may occur, and it shows how these secondary gammas are actually taken into account (see point 3, Fig. 1).

## 6. Detecting Emerging Photons

Once a particle emerges, its direction is checked to see if it hits the detector. The geometric details of the detection routine are given in Appendix E. If the particle is detected, its energy is recorded. This energy is used to compute the dose that tissue would receive, using the relationship:

$$D(\text{rad-cm}^2) = k(\text{gm-rad/MeV}) \cdot E_{\gamma}(\text{MeV}) \cdot \mu_a(E_{\gamma})(\text{cm}^2/\text{gm}) \quad (14)$$

where D is the dose due to that emerging particle, k is a units

conversion factor,  $E_\gamma$  is the gamma energy at the detector, and  $\mu_a$  is the mass absorption coefficient for tissue (a function of  $E_\gamma$ ). Eq. (14) calls for values of the mass absorption coefficients for tissue at all gamma energies of interest. This is done for the same energies and at the same point in the program where the various  $\mu$  components for each shielding material are input (at the beginning of the program). This absorption coefficient is given in tables and is found by subtracting the Compton scattering (excluding the small absorptive effect of such scattering) coefficient from the total mass attenuation coefficient,  $\mu$ , for tissue, at each energy in the charts.

#### D. Electron and Positron Tracking

##### 1. General Considerations

Enough basic theory has been discussed to be able to develop the computer program to find the buildup factors for gamma radiation. However, once this routine is prepared, it is relatively easy to extract information as to how the shield absorbs the energy removed from the incident gamma beam. This energy is transmitted directly to the photoelectron, the recoil Compton electron, and the positron-electron pair produced. These particles give up their energy through either ionization and excitation or re-radiation as bremsstrahlung emitted continuously along their path until they come to rest [3:127].

Studying the way in which the shielding absorbs the energy from the incident gamma beam may not appear to be germane to the calculation of buildup factors. But this is actually an important consideration in shielding design, and if this can be calculated within the

buildup factor program, it should be attempted. More importantly, these electrons (or positrons) emit bremsstrahlung as they pass through the shielding materials, with the effect most pronounced for the high Z materials and at high gamma energies. Bremsstrahlung gammas can contribute significantly to the scattered radiation. Thus, inclusion of the electron effects improves the accuracy of the buildup factor calculations and also yields additional information about the energy dissipation pattern.

To determine how this energy is distributed within the shield, the primary calculations are the determination of the range, energy, and direction of the electron or positron. Then, the portions of the slab affected can be identified, and the energy is distributed among the appropriate zones of the slab.

## 2. Electron Energy, Direction, and Range

Depending on the type of interaction in which the primary gamma was involved, the resulting electron or positron will be emitted with a certain energy and in a given direction. In the photoelectric effect, all the original gamma energy is assumed to be given to the emerging electron. In reality the electron energy is equal to  $E_{\gamma} - BE$ , where BE is the binding energy of the ejected electron. The binding energy will appear in the form of X-rays accompanying the photoelectric effect. These X-rays have energies in the keV range. They are readily absorbed, thus they do not affect the buildup factor values. The photoelectric process is assumed to be isotropic, so calculation of the particular electron vector from the point of interaction is straightforward.

In Compton scattering, the energy of the recoil electron ( $T_e$ ) is equal to that lost by the gamma-ray. The recoil angle ( $\theta_e$ ) is related to the angle through which the gamma was scattered ( $\theta_\gamma$ ) by the equation [1:676]:

$$\cot(\theta_e) = (1+\alpha) \tan(\theta_\gamma/2); \quad \alpha = E_\gamma/.511 \quad (15)$$

Since the recoil vectors for the gamma and electron form a plane, their azimuthal angles,  $\phi$ , will be  $180^\circ$  (or  $\pi$ ) apart. Hence:

$$\phi_e = \phi_\gamma + \pi \quad (16)$$

Again, both of these angles for the electron are measured in the local coordinate system.

The positron and electron formed in pair production are handled in a similar manner, except that now there are two particles depositing energy and re-radiating bremsstrahlung along different paths. The total energy of the original gamma is given up when pair production occurs. The energy ( $E_\gamma - 1.022$ ) MeV appears as kinetic energy of the two particles. The assumption used in the program is that this kinetic energy is shared equally by the positron and the electron. This assumption is good, because the maximum difference between the positron and the electron energies will occur at low gamma energies and amounts to about  $.0075Z$  MeV [1:704]. This difference decreases as the original gamma energy increases. For the highest  $Z$  considered (lead;  $Z=82$ ), this difference becomes a maximum of  $.615$  MeV. After assuming equal energies, conservation of momentum requires the respective angles of departure to be equal as well. Hence, the energy of either particle is:

$$T = E_p = E_e = \frac{1}{2} (E_\gamma - 1.022) \text{ MeV} \quad (17)$$

The local "scattering" angle is found to be quite small [1:703]:

$$\theta_p = \theta_e = .511/T \text{ radians; for } T \gg .511 \quad (18)$$

Since the positron and electron depart along two vectors which form a plane, their azimuthal angles are randomly distributed, but 180° apart. Hence, another random number,  $r$ , is generated to obtain:

$$\phi_e = 2\pi r \quad (19a)$$

$$\phi_p = \phi_e + \pi \quad (19b)$$

The energy and emerging direction of each type of electron can be determined for all possible events. The energy is needed to find the range, the amount of bremsstrahlung, and the amount of energy to be deposited within the shield. The direction is essential in using the calculated range to identify those portions of the shield in which the energy is to be deposited. Also, by determining the end point of the positron, this establishes the true point of annihilation. Thus, the latest positron coordinates are used as the birth point of the two annihilation gammas (see section II.C.5).

One final step in the determination of the electron vector is to convert the local cosines to cosines in the fixed coordinate system. Since an electron will only be tracked over a single range, and not over a sequence of distances as in the gamma tracking situation, only the current coordinate transformation matrix need be used to obtain the electron vector's direction with respect to the fixed system. Once the electron range is found, the end point of the electron vector

can be determined. Here the electron or positron comes to rest, having given up all its kinetic energy to the shielding material as either ionization and excitation, or as bremsstrahlung.

The range, when expressed in units of  $\text{gm/cm}^2$ , is, to a very good approximation, a function only of the electron energy (T), not the particular medium being traversed. The latter is taken into account when converting to an actual distance by dividing the material's density,  $\rho(\text{gm/cm}^3)$ , to get the range in cm. The energy, T, is uniquely determined for each type of electron for a given gamma history, and the range of the electron is calculated using the formula [2:242]:

$$R(\text{gm/cm}^2) = .412 T^{1.265-.0941\ln T}; \quad \text{for } T < 2.5 \text{ MeV} \quad (20a)$$

$$R(\text{gm/cm}^2) = .530 T - .106; \quad \text{for } T \geq 2.5 \text{ MeV} \quad (20b)$$

$$R(\text{cm}) = R(\text{gm/cm}^2) / \rho(\text{gm/cm}^3) \quad (20c)$$

The same range and energy deposition equations were used for both the positron and electron. This is valid when considering energies below 10 MeV [14]. Based on the material in which the electron starts, this "mass" range is converted to a "linear" range, using Eq. (20c). Then, with the known cosines for the electron vector, the end point for the electron path is established. Here, the electron comes to rest, and all its energy has been dissipated.

### 3. Energy Deposition

The geometric details of the energy deposition scheme are given in Appendix F.

For each electron the first task is to determine which materials, and which zones within those material regions, will be affected. The z coordinate of the end point of the electron vector is compared to the various region boundary values of z to determine which materials will be receiving the ionization energy. A loop is established to include all such regions. Then the affected zones within each region are found in a similar manner. This permits the establishment of an inner loop to compute the energy deposition over all affected zones in each region concerned. These energy deposition calculations are made for each zone in turn until all the electron energy has been distributed.

The energy given up in ionization can be expressed as [15:113]:

$$-\left(\frac{dE}{dS}\right)_{ion} = \frac{2\pi NZ E_0 r_0^2}{\beta^2} \left[ \ln \frac{(\gamma-1)\beta^2 E^2}{2I^2} + \frac{1}{\gamma^2} \left[ \frac{(\gamma^2-2\gamma+9)}{8} - (2\gamma-1)\ln 2 \right] \right] \quad (21)$$

where:  $N$  = atom density;  $Z$  = atomic number;  $E_0 = .511$  MeV;

$E = \gamma E_0 = T_e + E_0$ ;  $r_0 = e^2/E_0$  = classical electron radius;  $\beta = v_e/c$ ; and  $\gamma = (1-\beta^2)^{-1/2}$ . Since the energy is not deposited linearly with distance,

it is necessary to make an initial calculation for the first zone, remove the quantity of energy deposited from the available electron energy, and recompute a new amount of energy to be deposited in the next zone. The energy deposition using Eq. (21), can be expressed as:

$$\left| \frac{dE}{dS} \right|_{ion} = \frac{\Delta E_i}{\Delta S_i} = F(N, Z, \beta, I, E); \quad \text{or:} \quad \Delta E_i = (\Delta S)_i F \quad (22)$$

where the subscript,  $i$ , denotes the incremental energy and path length for the particular zone being considered. The computation of  $\Delta S_i$  for each zone is described in Appendix F. The basic Eq. (22) is applied



repeatedly for all affected zones. Each incremental energy,  $\Delta E_i$ , is stored in an accumulator indexed by zone number,  $i$ , and the type of electron or positron depositing that energy. When all interactions for each original gamma-ray history have been considered, these energy accumulators for each zone of the grid will provide the pattern of energy deposition within the shield.

#### 4. Bremsstrahlung

The primary purpose of considering electron processes was to obtain information on bremsstrahlung. When a charged particle is accelerated in an electromagnetic field, a certain amount of its energy is given up as "braking" radiation known as bremsstrahlung. This effect is a function of the particle's energy, the particular material being traversed, and the charged particle's mass [3:129]:

$$- \frac{dE}{dS}_{\text{rad}} = \frac{Z^2 E}{M^2} f(E) \quad (23)$$

Hence, although a proton also emits bremsstrahlung, it is about  $1840^2$  times more important for an electron of the same energy, since the electron is  $1/1840$  times less massive than the proton. As Eq. (23) shows, bremsstrahlung is important for the high  $Z$  materials, or for sufficiently high energy electrons in virtually any material. Hence, when studying gammas with energies initially of a few MeV, it is possible to neglect this additional gamma contribution to the buildup factor for low  $Z$  materials, but not for higher  $Z$  materials, such as lead.

Bremsstrahlung is emitted continuously along the path of the electron. The total amount of energy which is radiated is given by [1:615-617]:

$$E_b = 7 \times 10^{-4} Z E^2 \text{ MeV, for } E \leq 2.5 \text{ MeV} \quad (24)$$

Since the main program is set up to handle a finite number of gammas with discrete energies, the simplifying assumption is made that all the energy that the electron will emit as bremsstrahlung is emitted via a single gamma, at the point where the electron was produced, and in the direction of that electron. This assumption proves to be acceptable, since it considers all the energy re-radiated and leads to results which agree with experiments. Thus, directly from information already available for every electron, the bremsstrahlung emitted can be taken into account. Each of these gammas is well-defined, since its energy, initial coordinates, initial direction, and the material in which it starts are all known. Hence, eight parameters are stored for each bremsstrahlung photon produced: the material and energy at the point of emission, the three birth coordinates, and the three direction cosines (assumed to be identical with those of the parent electron).

The energy to be re-radiated as bremsstrahlung is calculated using Eq. (24) before entering the energy deposition scheme. Once the electron energy remaining to be deposited as ionization falls below this value of the energy to be re-radiated, the deposition routine must be terminated, even though the entire range of the electron may not have been traversed. Then the bremsstrahlung storage routine is

entered. After all primary gammas are studied, the bremsstrahlung radiation is considered in a second pass through the main program. This time, a new initialization sequence is followed, in which the eight stored parameters for a given bremsstrahlung particle are recalled for use.

It is practical to check the energy of the bremsstrahlung gamma before it is saved, to eliminate in advance those which will not survive in the second pass. The number of bremsstrahlung photons requiring storage may still be high, since one original gamma history can generate many bremsstrahlung photons. This fact may make possible a cascade effect, wherein 1000 original particles produce about 1700 secondaries, which during the second pass may produce many more bremsstrahlung. However, significantly less total energy will be available in successive generations of secondary photons. This is true because the bremsstrahlung-producing electrons or positrons are given only a fraction of the incident gamma energy at any one interaction. Of this electron energy, only a small percentage is typically radiated. It was found that the third and succeeding passes through the program did not add at all to the amount of radiation detected. Hence, a maximum of two passes (one for the original gammas, the second for the bremsstrahlung) was used. By using temporary storage areas on the computer, there was no need to allocate storage space for the bremsstrahlung data during the run of the program, hence there was practically no restriction on the amount of secondary radiation which could be considered on any run.

## E. Program Capabilities

### 1. Overall Considerations and Initialization

The program was written to be as flexible and general as possible. Only the laminar nature of the composite shield is fixed, thereby enabling concentration of the study along a principal coordinate axis,  $z$ , which is taken perpendicular to the face of the shield. The photons enter uniformly distributed over a circle having the desired beam area. In the case of normal incidence, the original direction of motion for each photon is parallel to the fixed  $z$ -axis.

It is relatively simple to tailor the beam to any particular need, such as a single energy or spectrum of energies, a parallel beam incident either normally or at some fixed angle, or an isotropic source. Also, the detector size and location are variable, and the transverse dimensions,  $x$  and  $y$ , of the slab can be selected independently.

Before the life histories of the gammas are processed, some preliminary details are considered. Frequently used coefficients are defined (see Appendix B), and the event counters are all initialized. The run control conditions described above are input on two data cards. The material properties of the shield, such as the attenuation coefficients ( $\mu$ ,  $\mu_c$ ,  $\mu_{pp}$ ) for discrete energies and other physical parameters, are input on six data cards per material. Next, the master loop is established to consider various thickness combinations within a single run of the program. In this multi-region framework,

it is then possible to establish equal-sized zones within each material to record the spatial distribution of the energy deposited within the shield. Then the study of the life histories begins. After the loop for all gamma histories in each case is completed, the results are tallied and analyzed.

## 2. Primary Results

The primary reason for developing this Monte Carlo program was to calculate the buildup factor. From Eq. (1), the buildup factor for a particular quantity is defined as [4:82]:

$$B = \text{total quantity (T)} / \text{uncollided quantity (U)} \quad (25)$$

The total quantity is made up of the collided (C) plus the uncollided (U) quantities, at the point in question within the shield, or beyond the shield. Hence:

$$B = T/U = (U+C)/U = 1 + C/U \quad (26)$$

In the case of gamma-ray attenuation, there are three distinct quantities which may be measured, and for which a buildup factor is meaningful. The simplest task is to measure the number buildup factor,  $B_n$ , wherein only the amount of particles penetrating the barrier is studied. But, due to the different effects particles of differing energies have on tissue, the total energy actually surviving in the emerging beam becomes a useful quantity to measure. This leads to the calculation of an energy buildup factor,  $B_e$ . Finally, the most practical application is in finding the dose buildup factor,  $B_d$ , since the dose is typically the quantity that the shield is designed to reduce. All of these buildup factors are calculated in this program.

Once a particle has emerged, it is tested for detection (see Appendix E). If the particle missed the detector, the event is recorded, and a new particle history is begun. If a detection occurs, then the particle history is sent from the scattering cycle to the detection routine. Here, the basic determination is whether the current particle has had an interaction within the shield. For this reason, a special counter is set at 0 at the start of each history and is increased by 1 for each interaction. If this counter is still zero when the detection routine is entered, the particle is uncollided. It retains its initial energy and direction, and the accumulators for uncollided number, energy, and dose imparted are incremented by the appropriate amounts. If the scattering counter is non-zero, then an interaction did occur, and the particle is a member of the scattered radiation. The energy of this gamma will have been reduced from its original value, hence the dose imparted (Eq. (14)) is also changed, because the  $\mu_{\text{abs}}$  for tissue is also a function of the photon energy on impact. These calculations are made, and the results are added to the accumulators for the collided number, energy, and dose imparted.

Getting the respective buildup factors is simple:

$$B_d = 1 + C_d/U_d \quad (27a)$$

$$B_e = 1 + C_e/U_e \quad (27b)$$

$$B_n = 1 + C_n/U_n \quad (27c)$$

The results also include the complete set of counters for each run, which tally the types of interactions and possible particle losses occurring by region, as well as the number of particles backscattered,

exiting the sides, emerging from the detector face, and those missing the detector.

### 3. Secondary Results

There are two "measurements" made by this program in addition to the buildup factor calculations. The more involved of these is the energy deposited within the shield as a function of the penetration depth. The major features of this routine have been described in detail in section II.D.3. Appendix F gives the pertinent geometric details. The results from the energy accumulators are displayed by material region. For each zone of the superimposed grid, the energy contribution of each component (photoelectron, Compton electron, positron, or pair production electron) is printed, with the total energy for a zone being the sum of these four contributions. Provision is also made for the grouping of zones, if desired, to reduce the number of points to be plotted. The full zone and grouped energy distribution patterns are then plotted by the computer for quick reference. Finally, the contribution made by secondary particles to the energy deposition scheme and the buildup factors is available directly from the output.

The other result obtained from the program is a description of the energy and spatial distribution of the original beam as it passes through the shield. This is accomplished at each region boundary of the shield. Two distribution matrices are assigned to each boundary, one for each direction that that interface can be traversed. Using the convention that odd interface numbers are for the positive  $z$

direction, interface #1 corresponds to the input face of the slab (see Appendix E). This "backscattering measurement" is another bonus of this routine, since this corresponds to the measurement of the number albedo of that material. The interfaces are numbered consecutively in this manner through the final face of the slab, where only the odd index number applies. Only those particles heading from the shield cross this interface. The opposite direction need not be considered, since no particle emerging from the back face of the shield will reenter.

For each particle as it crosses an interface, its energy and radial distance from the z-axis are calculated by the main routine. By dividing the energy and radial distance at the interface by a pre-designated  $\Delta E$  and  $\Delta R$ , respectively, the energy and radial groups can then be identified for this particle as:

$$\text{Energy Group: } IE = E_{\gamma}/\Delta E + 1 \quad (28a)$$

$$\text{Radial Group: } IR = R(\text{interface})/\Delta R + 1 \quad (28b)$$

The accumulators for these groups and this interface are each incremented by one. When the run is completed, a printout of all energy and radial groups provides a histogram for each interface, depicting the energy distribution and the radial dispersion pattern for the incident beam.

#### 4. Analysis of the Run

An analysis of these results is performed at the end of a particular run. The most important calculation is that of the standard error involved in the "measured" quantities. Both absolute and



relative errors are obtained. The theoretical basis for the error analysis is given in Appendix G.

The error in the buildup factor is a function of the error in each of its terms (C and U). In order to reduce the error, advantage is taken of the known exponential nature of the attenuation of uncollided radiation. The number of particles going through a thickness,  $t$ , without a collision is simply:

$$\text{Particles (Uncollided)} = N_0 e^{-\mu t} \quad (29)$$

where  $N_0$  is the total number of incident particles. Then the energy which will come through with this uncollided radiation is:

$$\text{Energy (Uncollided)} = N_0 E_0 e^{-\mu t} \quad (30)$$

Finally, the dose imparted by these particles is:

$$\text{Dose (Uncollided)} = N_0 E_0 k \mu_{\text{abs}} (E_0) e^{-\mu t} \quad (31)$$

Since each of these quantities is known exactly, there is no error introduced in the value of the buildup factor if these are used for the uncollided quantities in lieu of their values which are calculated in the program. In this way the error depends only upon the collided quantities. It should be mentioned, however, that the values of the uncollided quantities given by Eqs. (29-31) agree very well with the corresponding quantities calculated by the Monte Carlo routine.

The analysis of the results also includes an overall energy balance. Accumulators are established at the beginning of each run to keep track of the total energy input with the gamma-ray beam, the amount this beam loses to electrons and positrons through the three

types of interactions, the amount of energy these electrons and positrons actually deposit within the shielding materials, and the energy stored in the set of bremsstrahlung gammas. The total amount of energy remaining with the original gamma beam should equal the amount that is either detected or lost through all faces of the slab. The difference between the amount of energy received by the electrons and positrons and the amount actually deposited within the shield should equal the amount of bremsstrahlung produced. Finally, this routine demonstrates the magnitude of the bremsstrahlung effect, yielding the amount of energy considered, the amount neglected due to the individual gammas being of too low energy, and the amount neglected due to insufficient storage space. This last amount was zero for all cases studied.

#### 5. Checks Performed in the Development of the Program

At each stage in the development of the computer program, certain checks were made to insure that the simulation was correct. Many of these checks were temporary, but the most important of these were retained and the results included with the analysis for each run. Iron was selected as the best test material to be used in the development of the program. It is a medium Z material which has a representative set of attenuation coefficients. Hence, it does not waste histories by being too absorptive, as lead would. Also, with iron it is possible to have a significant amount of pair production to test that routine in the program, whereas the lighter materials, such as water or aluminum require an excessive number of histories to have much pair production.

One of the most critical calculations is of the anisotropic Compton scattering angle. Before the Kahn version of the rejection technique for the selection of the polar angle was implemented, the basic rejection technique was tried. Also, a table look-up scheme was developed using the Klein-Nishina formula. Elements of the table were the probabilities of scattering through various discrete angles for a range of energies. Each of these techniques yielded similar results, thereby providing a mutual check of each. For each of these methods, the frequency of selection of a particular angle  $\theta$  was printed out and plotted versus  $\theta$ . The resulting curve was the Klein-Nishina formula (Fig. 1). Kahn's method, being the most efficient, was adopted for the final program. In a related test, the program's response to a fixed scattering angle,  $\theta$ , was very good, with the buildup factor increasing significantly as the angle was forced to take on smaller values.

The angle of incidence of the beam was changed, and it was observed that the more oblique angle generally yielded lower buildup factors and an increased number of reflected particles [4:85].

Several runs were also made to find the best combination of beam and detector areas. It was found that a large beam coupled with a small detector (see Fig. 3) was equivalent to using a small beam with a large detector. The latter configuration was used because it makes more efficient use of computer time. Most of the scattered radiation emerging from the back face of the shield will be detected. This reduces the error of the final result for the same number of histories

studied. This also turned out to be the configuration used in the experiment which forms the basis for verifying the single material shield results [7].

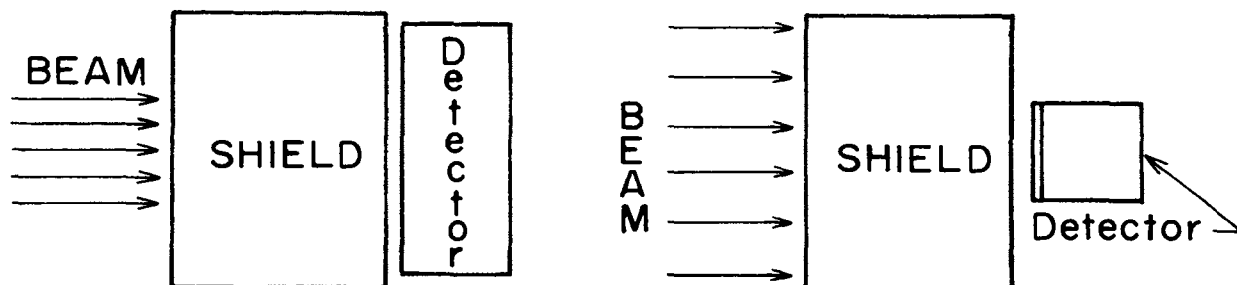


Figure 3: Two beam and detector size combinations considered

The computer's random number generator, which is crucial to a successful Monte Carlo simulation, was also checked. This was done by using a separate program to generate a large quantity of random numbers and checking their distribution over the range of values from zero to one. Running this routine every few weeks actually helped to disclose inadequacies in the generator which were later rectified.

The distribution of the selected distances between successive interactions was checked and found to be exponential, as it should be. The average distance for a given energy corresponded quite well to the known values of the mean free paths of the shielding materials at each energy.

To verify that the coordinate transformation was correct, a sequence of known distances and angles was introduced into the program, and the coordinates of the corresponding end points were calculated. The same calculations were performed by hand. The results were the same in both cases.

A most useful check system used in the program was a series of print options which displayed every pertinent variable in each computer routine for each history of a run. This proved to be most helpful in ascertaining that each portion was performing properly. Options for printing partial results and data from several key program routines have been retained in the final form of the code. Other permanent check features compute various averages. By keeping track of the very first distances and scattering angles chosen for each history, the average distance and average scattering angle corresponding to the fixed initial energy can be computed. To consider any distance or angle other than the first in this calculation would be wrong, since later interaction distances and angles are based on a spectrum of energies lower than the original one. The average distance travelled before the first interaction is equal to the mean free path. The average scattering angle increases as energy decreases. A final average of interest is the number of interactions each collided particle has had before it emerges and is detected. This roughly increases with increasing thickness, thereby providing another check on the reliability of the results.

Several counters are used to keep track of all the events which occur in each region and the ultimate fate of each particle. These are displayed so that any discrepancy is easily detected. Finally, as a check for the multi-layer systems, the interface data for the energy and radial distributions were printed out and found to have the expected values.

### III. RESULTS AND CONCLUSIONS

#### A. Buildup Factor Results

##### 1. Cases Considered

The computer program was used in the study of a certain number of cases, with the following conditions kept constant throughout the work:

- a. Beam area =  $1 \text{ cm}^2$  (circular).
- b. Angle of beam incidence =  $0^\circ$ .
- c. Detector area =  $3720 \text{ cm}^2$  (circular).
- d. Distance between detector and back face of shield = 0 cm.
- e. Transverse dimensions of the shield:  $x = y = \pm 100 \text{ cm}$ .
- f. Maximum number of scatterings allowed per history = 100.
- g. Minimum energy = .01 MeV = 10 keV.
- h. Nominal zone size for electron energy deposition = .1 cm.

The variables for each run were the initial gamma energy, the number of histories to be considered, and the shielding materials and thicknesses. Limitations e and f above were never exceeded.

The first priority was given to calculating buildup factors for a single material region, because experimental results corresponding to the specific source and shielding geometry of the program exist [7]. Thus, direct verification of the program was possible. With the program functioning properly for single regions of both medium and high Z materials, the study of a two layer shield began. Comparison was made with other Monte Carlo calculations [8] made at 1 MeV.

Finally, the buildup factor calculations were extended to higher energies, where the effects of secondary gammas is more pronounced.

## 2. Single Material Shields

Experimental results [7] for dose buildup factors are available for iron and lead shields at gamma energies of 6 and 8 MeV. Figure 4 gives the results for iron ( $Z=26$ ). This is an example of a medium  $Z$  material, for which the bremsstrahlung contribution is not significant. Therefore, the correlation between these experimental results and the Monte Carlo calculations was made without having to consider bremsstrahlung photons. Annihilation photons were considered in all cases studied.

However, matching Monte Carlo results for lead ( $Z=82$ ) with experimental values, disclosed the need to consider bremsstrahlung photons. Figure 5 shows, for 6 and 8 MeV gammas in lead, four different values for the dose buildup factors as a function of shield thickness:

- a. Experimental results [7], with a maximum error of 15%.
- b. Moments method results [7], which do not include either annihilation or bremsstrahlung photons.
- c. Results of the present work, using only one pass through the program, therefore excluding bremsstrahlung.
- d. Results of the present work, including bremsstrahlung considered in a second pass through the program.

The error in the present Monte Carlo calculations was kept below 12 percent in all cases, with most of the results having an error of

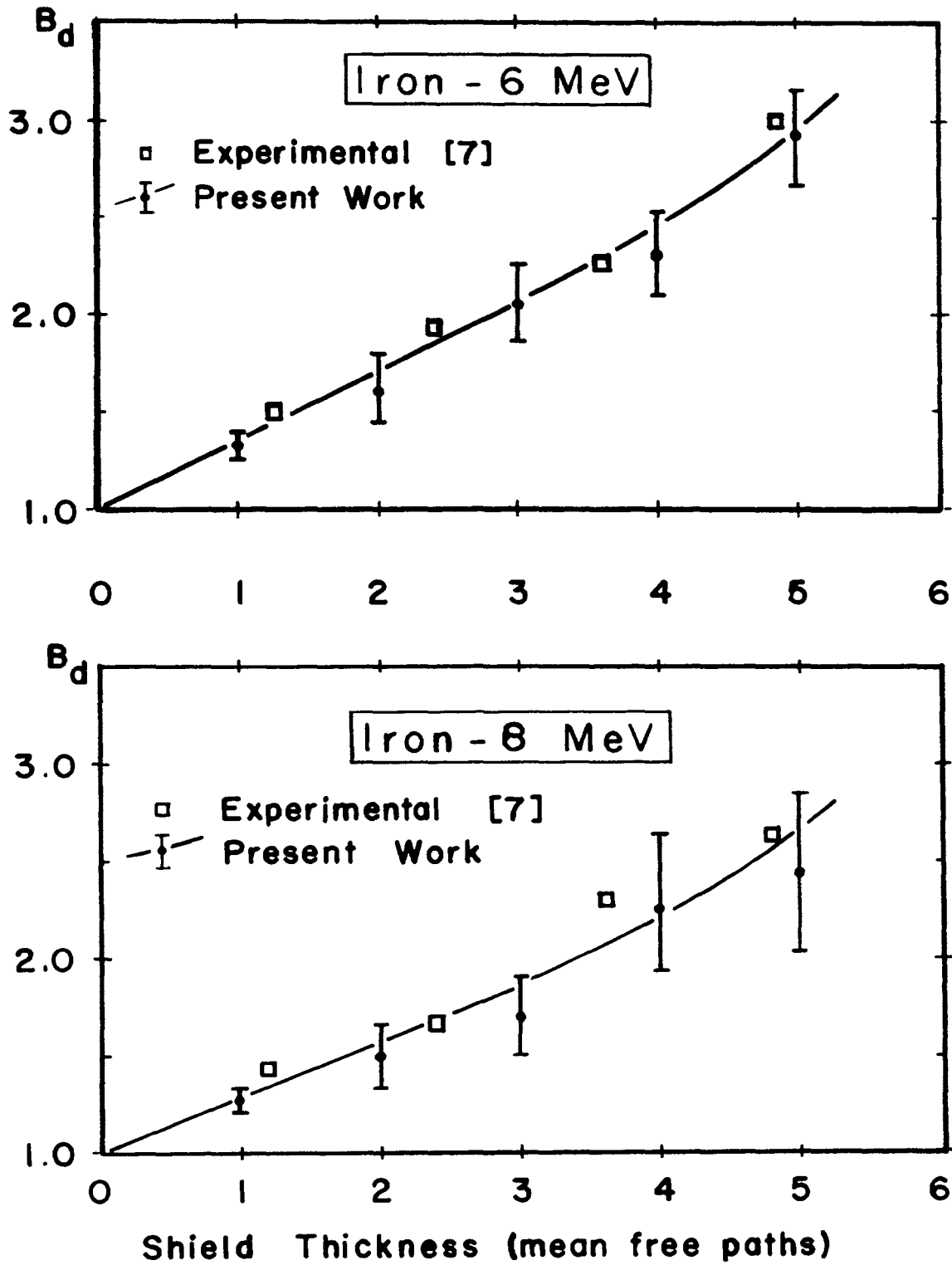


Figure 4: Dose buildup factors for single material (iron) shields, as a function of thickness, at gamma energies of 6 and 8 MeV.



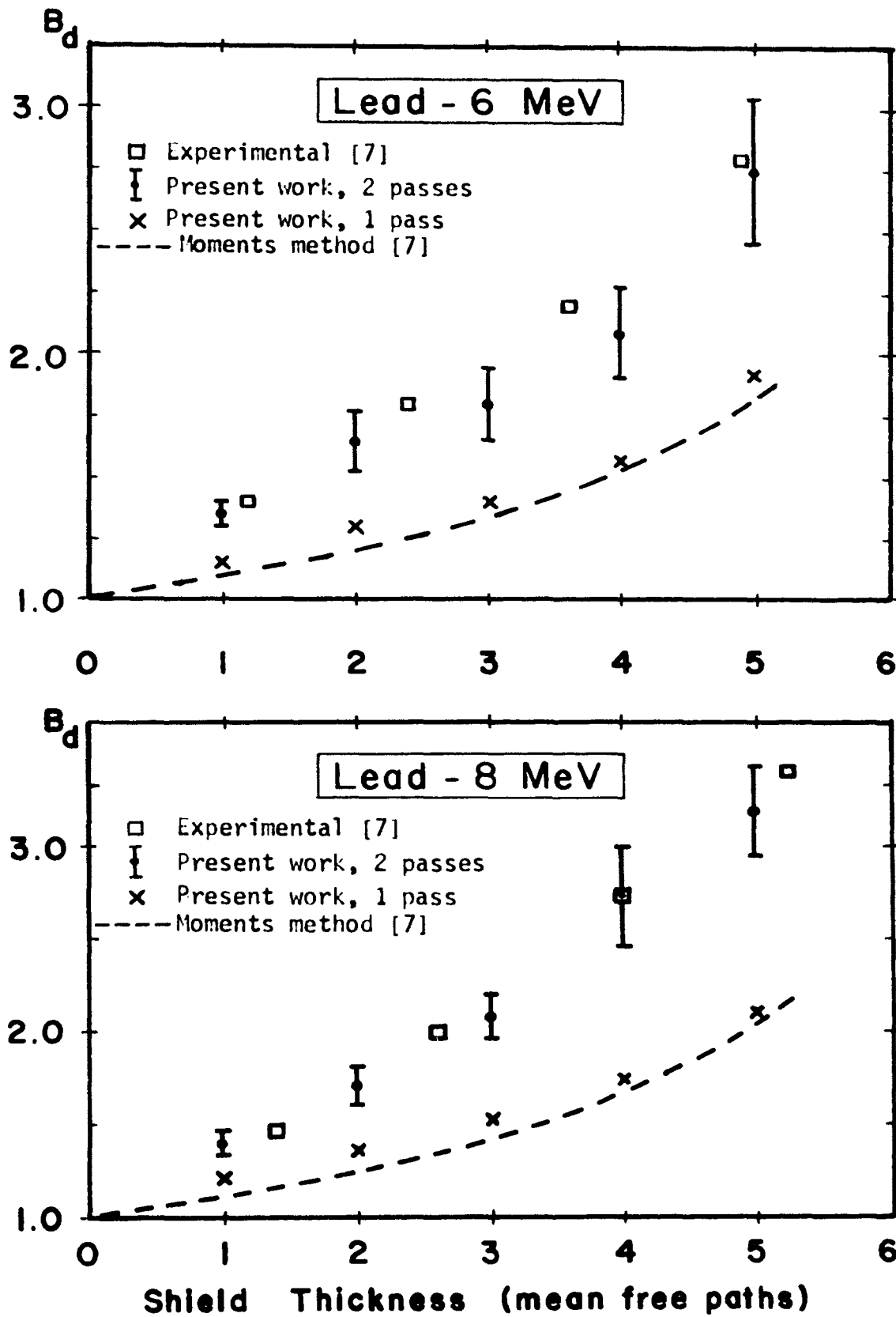


Figure 5: Dose buildup factors for single material (lead) shields, as a function of thickness, at gamma energies of 6 and 8 MeV.

8 percent or less. Achieving such good agreement between the Monte Carlo calculations and experimental results for a high Z material, such as lead, was the most significant accomplishment of this work.

Analysis of the single region results is straightforward. The typical pattern is for the buildup factor to increase with increasing incident gamma energy. Also, for a constant energy, the buildup factor decreases with increasing Z of the shielding material. This is true basically at energies low enough so that secondary processes are insignificant. Figure 5 supports the energy trend, with the buildup factors for lead being higher at 8 MeV than at 6 MeV. However, the results at either energy for iron and lead are fairly close to each other. The iron at lower energies would normally have a higher buildup factor. But, with the amount of bremsstrahlung produced being a function of  $Z^2E$ , at 8 MeV and for the same thickness in mean free paths, the dose buildup factor for lead is higher than that for iron. It should be pointed out, that the same thicknesses in mean free paths (mfp) are physically different (in centimeters) for different materials. For example, at 8 MeV, 5 mfp of iron is a physical thickness of 21.6 cm, whereas 5 mfp of lead is 9.6 cm.

### 3. Double Material Shields

Lead and aluminum, with a total thickness of four mean free paths, were selected for the study of double material shields. These materials were chosen because they offer the most contrast of low and high Z. By considering a thickness of 4 mfp instead of 6 mfp (for

which published results also exist), a relatively low number of incident particles gave acceptable accuracy for the results. Obviously, any thickness could be studied, if one is willing to accept the increase in computer time.

The double layer shield was studied for three incident gamma-ray energies: 1, 4, and 8 MeV. These energies correspond respectively to: a low energy case, for which pair production does not occur and bremsstrahlung is insignificant; a middle energy case, in which both annihilation and bremsstrahlung contribute to the buildup factors; a high energy case, where secondary gammas contribute appreciably to the results. Figures 6 and 7 show the energy and number buildup factors at each energy. The 1 MeV case provides a comparison between the current work and previous Monte Carlo calculations [8]. Only number and energy buildup factors are presented in reference 8. Figure 8 presents the dose buildup factors obtained from the three energy cases. The dose buildup factors are the most meaningful in studying the shielding properties of materials. Next in importance are the energy buildup factors. The number buildup factors merely reflect the number of particles which succeed in traversing the full thickness of a given shield, whereas the dose and energy buildup factors provide information on the quality and effects of such radiation.

A curve fitting technique was considered for this data. However, this would not add to the accuracy of the calculated results. Also, obtaining a "best fit" curve would be more appropriate if a semi-empirical equation were to be developed, which was not the case in the

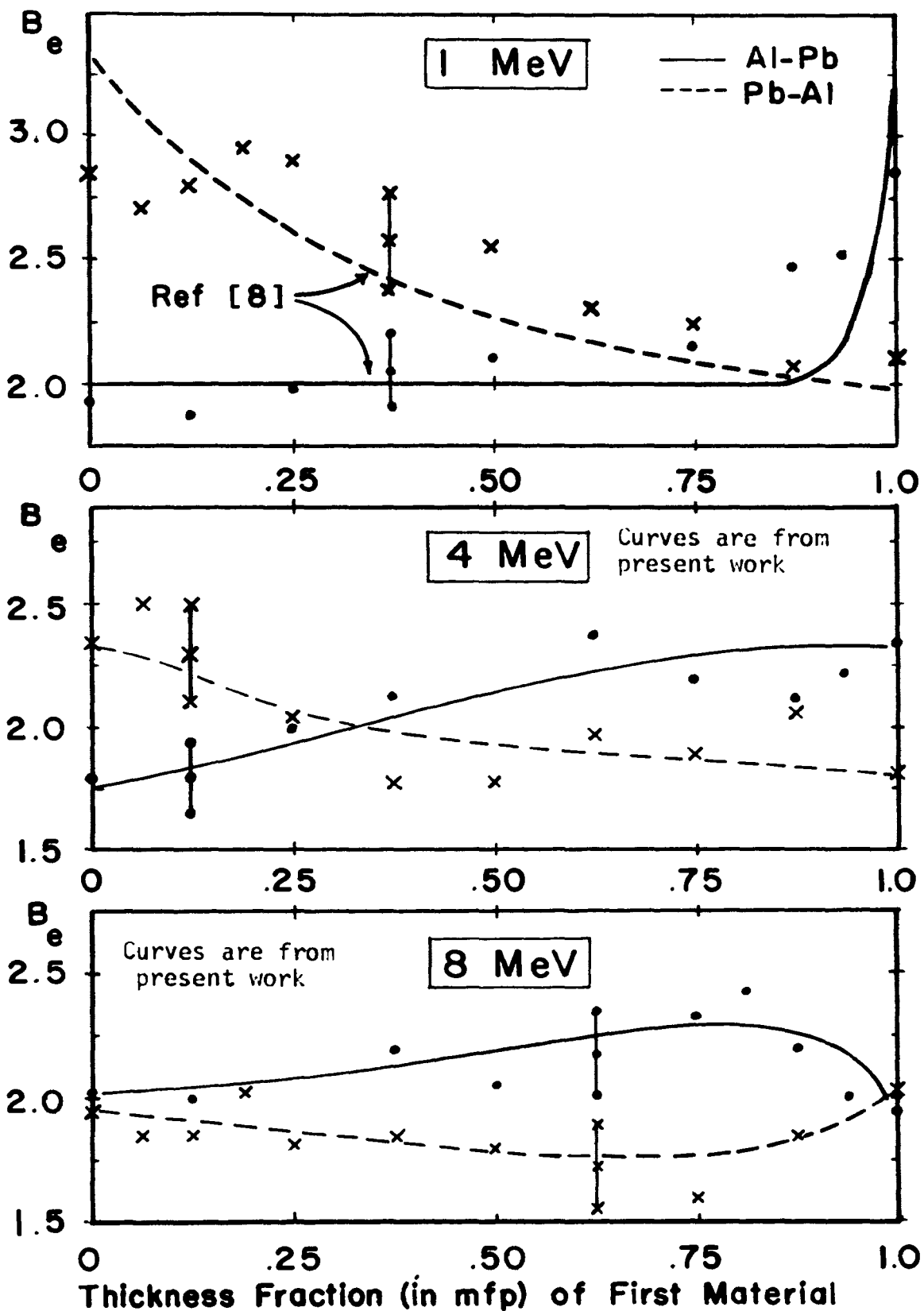


Figure 6: Energy buildup factors for 4 mfp of a composite shield of aluminum and lead, at gamma energies of 1, 4, and 8 MeV.

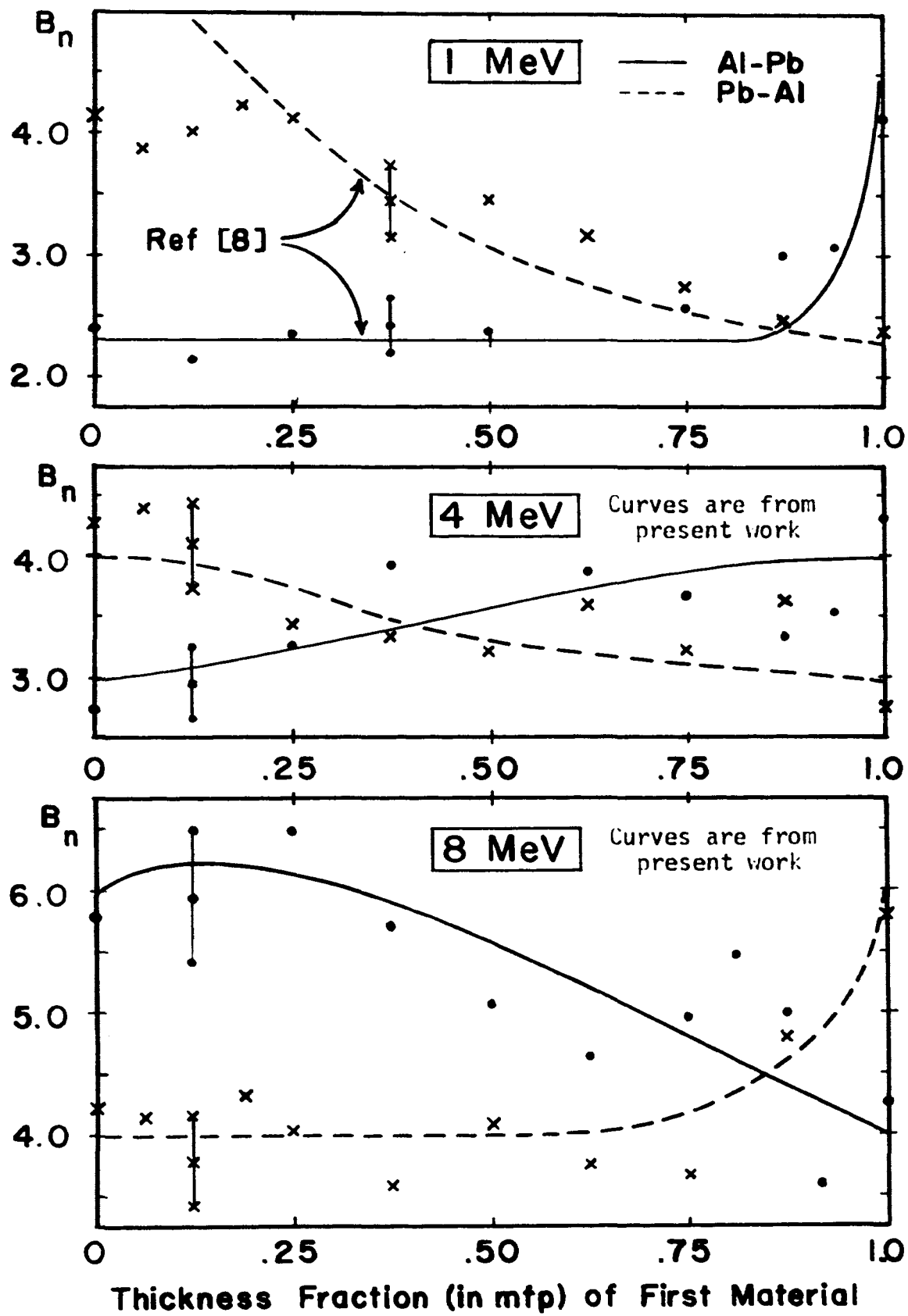


Figure 7: Number buildup factors for 4 mfp of a composite shield of aluminum and lead, at gamma energies of 1, 4, and 8 MeV.

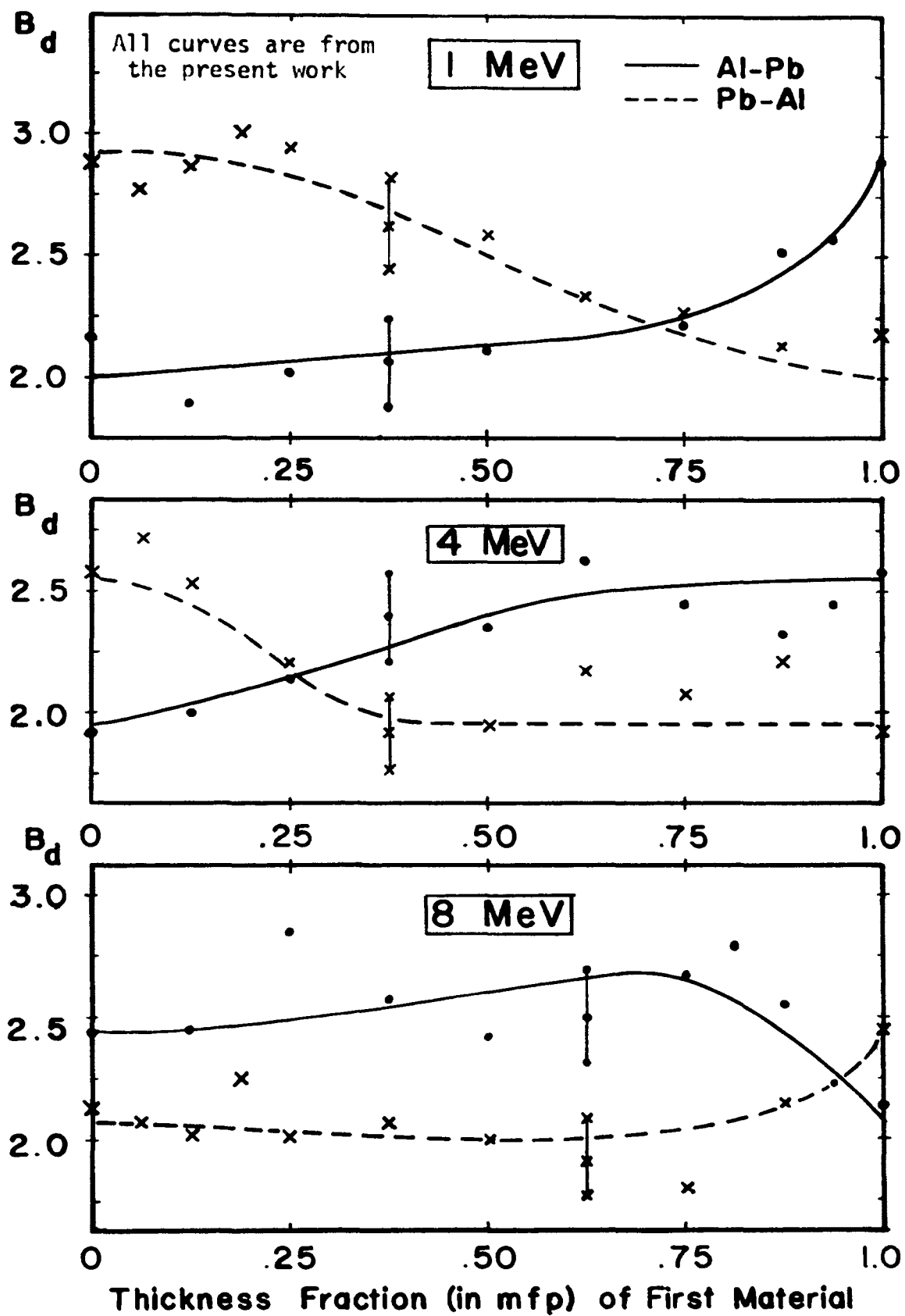


Figure 8: Dose buildup factors for 4 mfp of a composite shield of aluminum and lead, at gamma energies of 1, 4, and 8 MeV.

present work. Hence, all curves (except for  $B_e$  and  $B_n$  at 1 MeV) were drawn freehand. For clarity, the error bars are not shown for each point, but a single representative error bar is given for each curve.

The 1 MeV results clearly show a well defined trend, but the higher energy graphs are more difficult to interpret. At 1 MeV, the shield with the Al-Pb configuration has a fairly constant buildup factor, until the aluminum comprises 75 percent of the shield (in units of mfp). After that point, the values quickly rise to that of pure aluminum. Aluminum is a high scattering medium, whereas lead is highly absorptive. With aluminum the first shielding material, most of the gammas will reach the lead region, where they will be absorbed more readily. Hence, the composite shield behaves much like 4 mfp of pure lead. When the materials are reversed (Pb-Al), once the gammas traverse the lead, they stand a better chance of emerging from the aluminum. Hence, the buildup factors for that shielding arrangement are slightly higher in the middle range (25-75 percent). Certainly, there should be no appreciable difference at the extremes of each case, since the buildup factor for 100 percent aluminum in the Al-Pb shield should be equal to the original point (0 percent lead) for the Pb-Al curve, and vice versa. The fact that the results of this work satisfy this requirement, for each buildup factor and at all energies considered, is an additional check of the correctness of the program.

At 4 and 8 MeV, the trends are less obvious. Again, the buildup factors with aluminum as the second material are higher in the middle range than is the case when aluminum is placed first in the shield.

However, there is no discernible trend as remarkable as the sharp rise in the Al-Pb curves at 1 MeV.

## B. Secondary Results

### 1. Energy Deposition

Several representative cases were selected for investigation of the energy deposition patterns within various shields. To get a contrast, initial gamma energies of 1 and 8 MeV were run. Again, the materials were lead and aluminum with a total shielding thickness of 4 mfp. The cases studied were: all aluminum, all lead, 2 mfp each of Al-Pb and Pb-Al. The results for 1 MeV are presented in Figure 9 in terms of the physical dimensions of the shield (cm) in semi-logarithmic form.

No real difference was detected between the two energies studied. However, two distinct trends were noted for the materials used. Within a given material, the energy from the electrons is deposited in basically an exponential manner, hence the use of the semi-log plot. This is to be expected, since an electron or electron-positron pair results from each interaction between the gamma-rays and the shielding material, and the location of successive interactions is exponentially distributed.

For the double region shields, with lead placed second, there is a sharp rise in the energy deposited once the lead is encountered. In aluminum, Compton scattering dominates, hence the amount of energy transferred from the gamma-ray to the electron is relatively low.



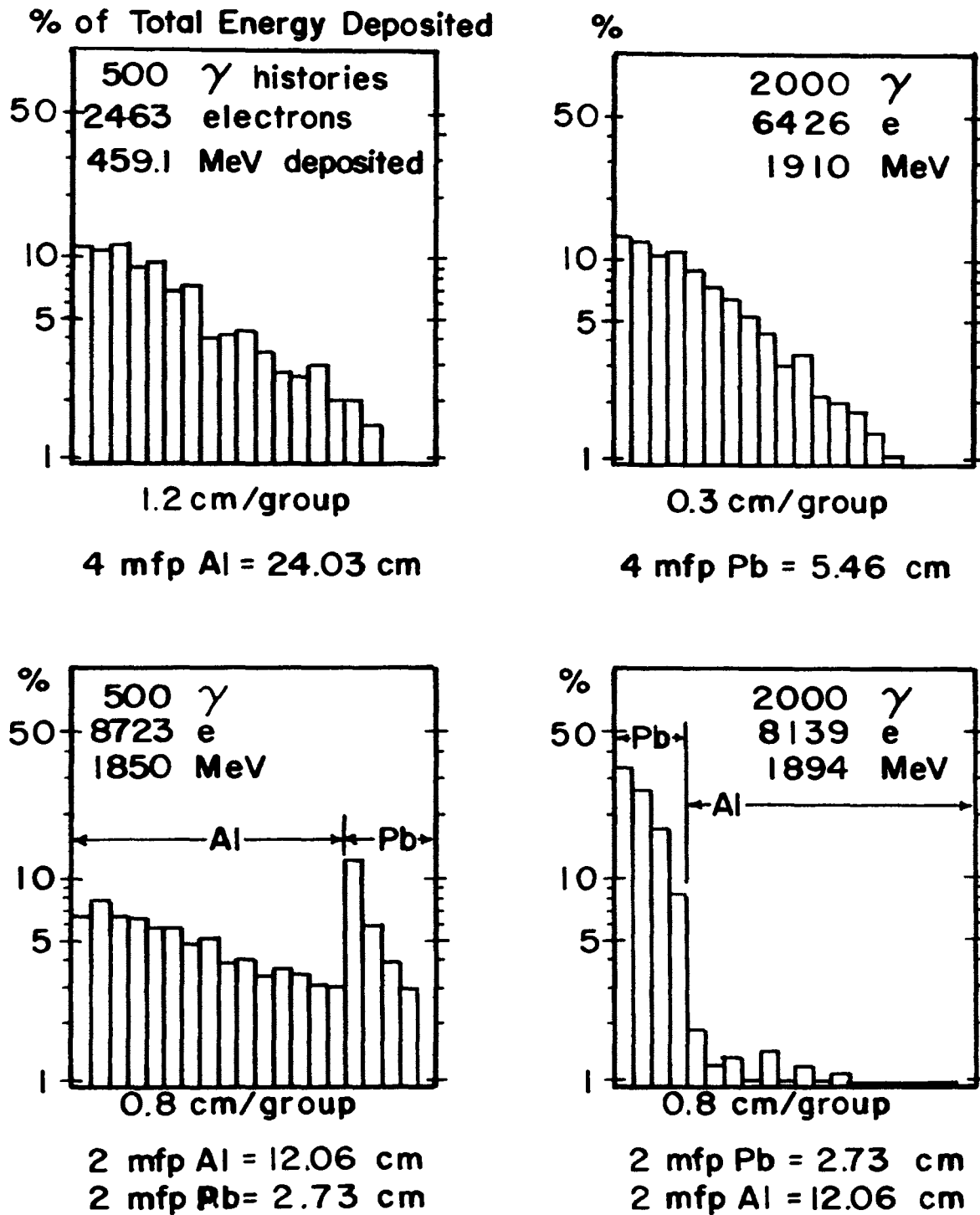


Figure 9: Various energy deposition patterns in lead and aluminum shields at 1 MeV.

When the highly absorptive lead region is entered, the photoelectric effect dominates, with the gamma giving up all its energy to the electron. When the lead comes first, no such jump occurs, since the aluminum does not cause much photoelectric effect to occur. Hence, the second layer of aluminum does not produce enough highly energetic electrons to cause a peak in the energy deposition curve. Another reason for the jump which occurs in the first few centimeters of lead is the difference in physical scales involved in converting from mfp units to centimeters. The 2 mfp thickness of aluminum is more than four times as thick in centimeters as 2 mfp of lead, at an initial gamma energy of 1 MeV. Since Figure 9 is based on the real scale (cm), the effects of lead are much more compactly depicted.

## 2. Energy and Spatial Distributions of Gammas at Interfaces

The results after each run include the energy and radial distributions for the gamma-rays at each interface of the shield. For convenience and easy comparison, the energy and radial spectra were subdivided into twenty energy groups. The energy spectrum thus ranges from zero to  $E_0$ , the initial gamma energy for the run. The radial group size was set at 1 cm for all runs. Thus, the radial distance,  $r$ , ranged from zero to 20 cm. All particles crossing the interface with radial distance greater than 20 cms were counted with the final group (19-20 cm).

Figure 10 shows the interface numbering system. Interfaces 1, 3, and 5 are for the incident, Al-Pb, and final interfaces traversed in the positive  $z$  direction. Interface 2 counts those particles

reflected from the Al layer, hence are reflected from the incident face of the slab shield. Interface 4 counts particles leaving the second material (Pb) and returning to the first (Al).

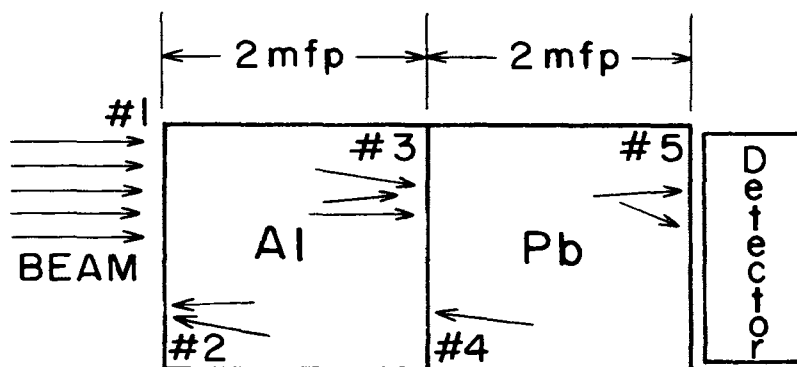


Figure 10: Interface numbering system used in the energy and radial distributions for gamma-rays

Figure 11 presents typical results for a run of 2 mfp Al and 2 mfp Pb at 1 MeV in semi-log form. All the particles start out with  $E_0$  within  $r \leq 1$  cm, hence the histograms for interface 1 count all 2000 incident particles in a single energy and radial group. At interface 3, the number remaining in the original groups ( $E = E_0$ ;  $r \leq 1$  cm) is decreased by approximately a factor of  $e^2$ , due to the attenuation occurring in the two mean free paths of Al. Another such decrease also occurs at interface 5, after 2 mfp of lead. The reverse interfaces also demonstrate reasonable results. If a particle is back-scattered from the first region, it will have lost most of its energy. Hence, we would expect none of these backscattered particles to have very high energies. This is what the interface 2 energy distribution shows. Interface 4 depicts the same effect, only the number of particles has been decreased substantially. The spatial distribution

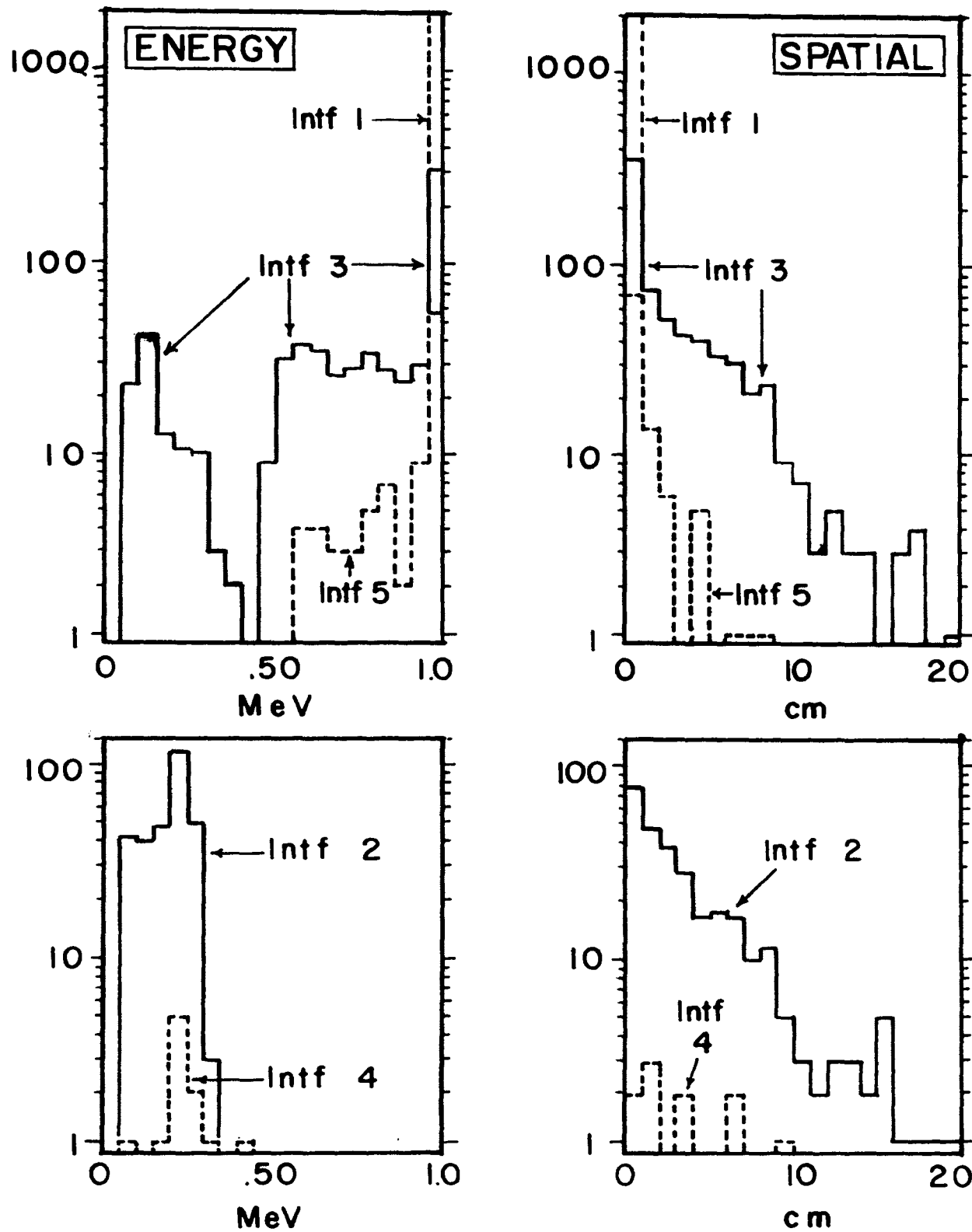


Figure 11: Energy and spatial distributions at each interface of an Al-Pb shield at 1 MeV for 2000 original gamma-rays.

in all cases demonstrates the exponential manner in which the beam spreads radially as it progresses through the shield.

### C. Conclusions

This work has achieved its objective of calculating buildup factors for multi-layer shields using the Monte Carlo method. The calculated values for single material shields are compatible with experimental results. These calculations amply demonstrate the need to consider secondary gammas when working with high Z shielding materials and a high incident gamma-ray energy. The double material shield results also are in agreement with previous calculations in this field. Extension of the two layer shielding study to higher energy cases yields an inconclusive buildup factor pattern, indicating that more work is required, if a semi-empirical formula is to be developed.

The ancillary results, such as the energy deposition pattern and the interface distributions, provide valuable information on the properties of the shielding materials studied. They also serve to substantiate the validity of the Monte Carlo simulation, thereby increasing the confidence in the buildup factors obtained. The value of the computer program is also enhanced by the general nature of most of the routines, making the code readily adaptable to the study of a wide variety of shielding situations.

The experience gained in the course of this investigation leads to two overall conclusions concerning the Monte Carlo approach. There are a great many ways errors may be introduced into the program

without being detected. Therefore, checks must continually be made, and great care must be taken in applying the theory to the computer coding. Secondly, the Monte Carlo method can be used to yield results as good as other calculating techniques and often can be applied to cases beyond the limits of any other approach, especially for complicated geometries.

#### D. Recommendations for Further Work

This investigation has been restricted to a certain area of study: the calculation of buildup factors for a monoenergetic gamma-ray beam, normally incident upon a slab shield of several distinct material regions. But the program which has been developed is much more powerful, since it can be used to study other situations with little or no modification. There are four general areas of application where such extension of the present program is possible: the incident beam, the shielding geometry, the shielding composition, and the parameters to be studied.

The incident beam can have a spectrum of energies and impinge on the shield at any angle. A point isotropic source or system of sources could be studied. A spectrum of energies poses no real problem either. Currently, a single initial energy value is introduced and used for each history. However, an energy spectrum could be studied with the addition of a routine which selects input energies according to the desired spectrum.

The shielding geometry used here was a slab. This fixes the critical thickness parameter along a principal axis ( $z$ ), with two

transverse directions ( $x$  and  $y$ ). To go to cylindrical or spherical geometry, all the geometric transformations should be rewritten in terms of the new geometry. This could be done with minimum difficulty.

Variations in the shielding composition is another interesting and practical research area. Different combinations of pure elements or more useful alloys could be tested. Most of the adjustments would be in obtaining or preparing the input data for such materials. As discussed above for different geometries, even the slab case could consider variations in the shielding properties in the transverse dimensions,  $x$  and  $y$ . These may be different materials or the same material but with differing consistency or thickness laterally. Another possibility would be the study of the effects of void regions or ducts penetrating the shield in some configuration. This would be a most practical investigation, since most physical shields must be designed with some access ports or ducts for equipment, instrumentation, cooling systems, and so forth.

Finally, the very parameters which are to be measured can vary greatly. This work centered on the buildup factor calculations but touched upon the following related topics: the pattern of energy deposition within the shield, changes in the beam's energy and spatial distributions as it passes through the shield, and the number albedo at the incident face. Clearly, each of these topics could be studied in much greater detail, both for the multi-region and single-region shields. By reducing the system to a single material region, each of these parameters could be calculated more efficiently, and the results

would definitely be attributable to a single material. To study the energy and radial distribution patterns in the single region case in greater detail, one can simply cause the "interfaces" to be numbered at each energy deposition zone boundary, thereby giving a much better resolution for the changing energy and spacial parameters. Also, based on the energy dissipation scheme, channels may be required at certain depths within the shield to permit coolant flow. This practical aspect of the design could be simulated. Finally, albedo calculations could be made using this program. Since there are three common components of this reflection parameter (dose, number, and energy), one could find these albedos as a function of the incident energy, the incident angle, and various combinations of backscattering materials.



## BIBLIOGRAPHY

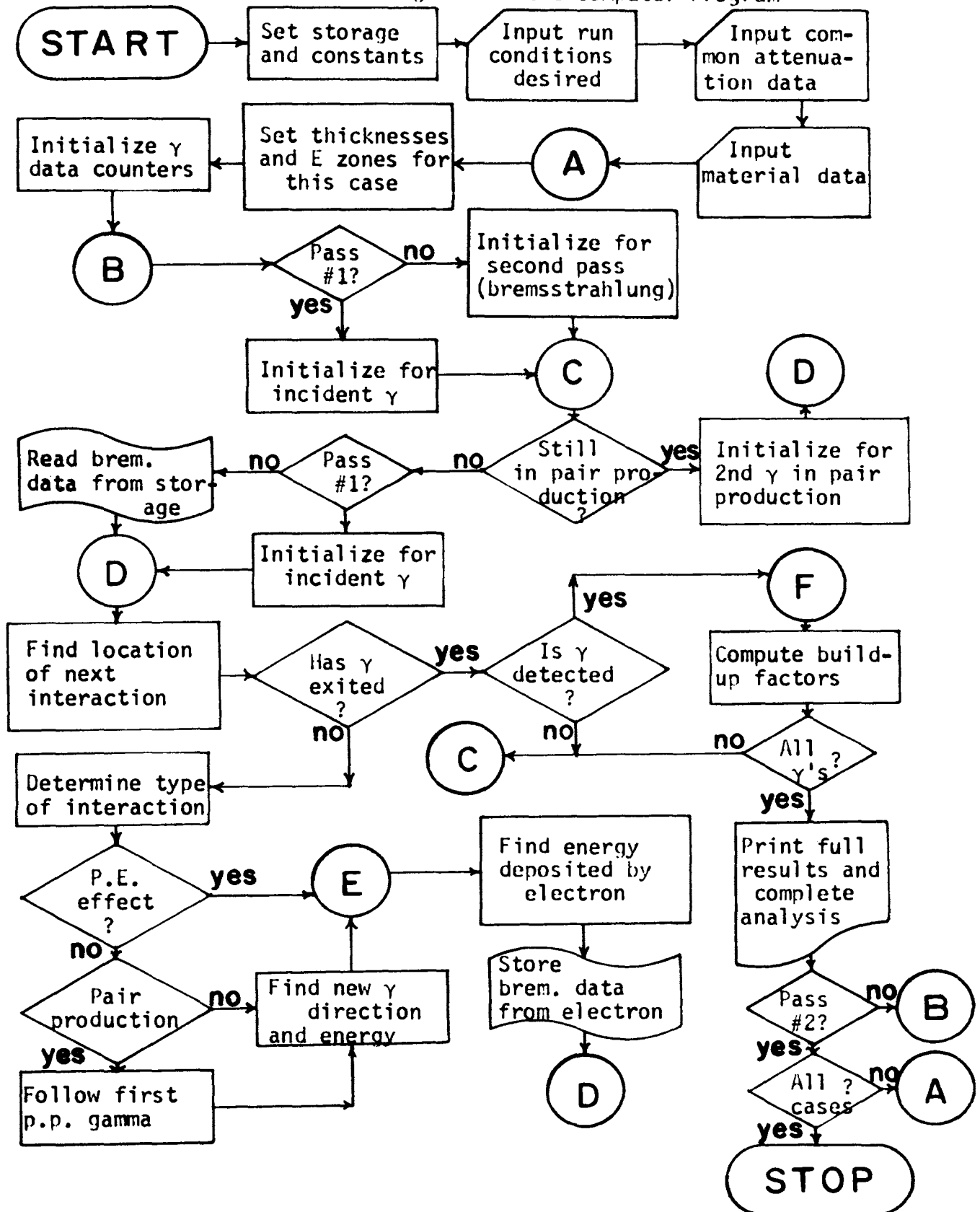
1. Evans, Robley D. The Atomic Nucleus. New York: McGraw-Hill Book Company, Inc., 1955.
2. Arya, Atam P. Fundamentals of Nuclear Physics. Boston: Allyn and Bacon, Inc., 1966.
3. Heckmann, Harry H., and Starring, Paul W. Nuclear Physics and the Fundamental Particles. New York: Holt, Rinehart and Winston, Inc., 1963.
4. Kazanskii, Yu. A., and others. Physics of Reactor Shielding. Jerusalem: Israel Program for Scientific Translations, 1969.
5. Goldstein, Herbert. Fundamental Aspects of Reactor Shielding. Reading, Massachusetts: Addison-Wesley Publishing Company, Inc., 1959.
6. Jaeger, R. G. (ed.). Engineering Compendium on Radiation Shielding, Vol 1: "Shielding Fundamentals and Methods". New York: International Atomic Energy Agency, 1968.
7. Johnson, W. Reed, and others. "Gamma Ray Attenuation at Energies of Approximately 6 and 8 MeV," Nucl. Sci. Eng. 43, 32 (1971).
8. Steyn, J. J., and others. "Gamma Photon Buildup Factors and Albedos for Finite Laminar Shields," ANS Transactions 14, 890 (1971).
9. Shirkin, L. M. "Use of the Monte Carlo Method for Calculating the Penetration of Gamma Radiation through Matter," Sov. At. En. 17, 1279 (1964).
10. Pozdneev, D. B. "Dose Buildup Factors for Low Energy Gamma Rays in Homogeneous and Heterogeneous Barriers," (Abstract Only), Sov. At. En. 21, 851 (1966).
11. Spanier, Jerome, and Gelbard, Ely M. Monte Carlo Principles and Neutron Transport Problems. London: Addison-Wesley Publishing Company, Inc., 1969.
12. Kahn, Herman. "Applications of Monte Carlo." Rand Corporation Research Memorandum, RM 1237-AEC, 19 April 1954, revised 27 April 1956.
13. Gaggero, G. "Monte Carlo Calculations for the Photofractions and Energy Loss Spectra of Ge(Li) Semiconductor Detectors," Nucl. Instr. Meth. 94, 481 (1971).

14. NASA SP-3012. Tables of Energy Losses and Ranges of Electrons and Positrons, M. J. Berger and S. M. Seltzer, 1964.
15. Roy, R. R., and Reed, Robert D. Interactions of Photons and Leptons with Matter. New York: Academic Press, Inc., 1968.
16. NBS Circular 583. X-ray Attenuation Coefficients from 10 KeV to 100 MeV, G. W. Grodstein, April 30, 1957.
17. Lamarsh, John R. Introduction to Nuclear Reactor Theory. Reading, Massachusetts: Addison-Wesley Publishing Company, Inc., 1966.
18. Handbook of Physics and Chemistry. 50th Ed. Cleveland: Chemical Rubber Company, 1969.
19. Caldwell, D. O. "Range-Energy Relation and Masses of the New Particles," Phys. Rev. 100, 291 (1955).
20. Standard Math Tables. 19th Ed. Cleveland: Chemical Rubber Company, 1971.
21. Kalter, Charles J. Private Communication. May 1971.
22. Faddeev, D. K., and Faddeeva, V. N. Computational Methods of Linear Algebra. San Francisco: W. H. Freeman and Company, 1963.
23. Glasstone, Samuel, and Sesonske, Alexander. Nuclear Reactor Engineering. Princeton: D. Van Nostrand and Company, Inc., 1967.
24. Price, William J. Nuclear Radiation Detection. 2nd Ed. New York: McGraw-Hill, 1964.
25. Melissinos, Adrian C. Experiments in Modern Physics. New York: Academic Press, 1966.
26. ANL-5800. Reactor Physics Constants. Argonne National Laboratory, United States Atomic Energy Commission, Washington, D.C., 1963.

## VITA

John Paul Kuspa was born in Detroit, Michigan, on January 13, 1946. He received his primary education in Detroit and his secondary education in Southgate, Michigan. He attended the United States Military Academy at West Point, New York, receiving the Bachelor of Science degree in June 1967. Since graduating from the academy, he has been on active duty as an officer in the United States Army, with tours of duty in Pirmasens, Germany; Fort Riley, Kansas; and the Republic of Vietnam. He has been enrolled in the Graduate School of the University of Missouri-Rolla since September 1970.

Appendix A: Block Diagram for the Computer Program



## APPENDIX B

## DATA USED

## 1. Shielding Material Properties

Table 1 is a chart of the various physical parameters required for each of the materials for which data was sought. Iron was used in the development of the program for a single material region. Aluminum and lead were used in the study of double layer shields. Data for water is included for convenience, since it is another common shielding material.

Table 1: Material Properties

Quantity	Symbol	Units	H <sub>2</sub> O	Al	Fe	Pb	Reference
Atom Density	N	10 <sup>24</sup> cm <sup>-3</sup>	.0334	.0602	.0847	.0335	[17:558-561]
Mass Density	ρ	gm/cm <sup>3</sup>	1.00	2.70	7.86	11.34	[18:B83-B120]
Atomic Number	Z	-	(6.6)*	13	26	82	[18:B10-B29]
Atomic Mass	A	amu	18.02	26.98	55.85	207.19	[15:B271-B499]
Ionization Potential	I	eV	74	180	365	1136	[19]

\*Calculated from equation given in [1:631].

Classical Electron Radius:  $r_0 = 2.818 \times 10^{-13}$  cm

Dose Conversion Factors: 1 MeV =  $1.602 \times 10^{-6}$  ergs

1 rad = 100 ergs/gm; hence,  $k = 6.24 \times 10^7$  MeV/(gm-rad)

## 2. Attenuation Coefficients ( $\mu$ )

Coefficients were required for tissue and the four shielding materials considered. Tables 2 and 3 give these values. The only difficulty which arose in developing this data is that some of it is in graph form, the rest is either in tables or not given at all. For elements not given explicitly, conversion from known values for other elements must be made. Let  $x$  and  $y$  be the subscripts of the unknown and known data, respectively. Then, for Compton scattering, one can convert from one element to another by [1:686]:

$$\mu_x/\mu_y = N_x Z_x / N_y Z_y \quad (32)$$

where  $N$  and  $Z$  can be obtained from Table 1. Since  $N = \rho N_a / A$ , where  $N_a$  is Avagadro's Number ( $6.023 \times 10^{24}$  atoms/gm-mole), we can get the value for the mass attenuation coefficient ( $\mu_c$ ) from:

$$\mu_c = \mu_x / \rho_x = \mu_y Z_x A_y / \rho_y Z_y A_x \quad (\text{cm}^2/\text{gm}) \quad (33)$$

The Compton values for aluminum were used to obtain those for iron.

For pair production, the conversion is similar [1:707]:

$$\mu_{pp} = \mu_x / \rho_x = \mu_y A_y Z_x^2 / \rho_y A_x Z_y^2 \quad (\text{cm}^2/\text{gm}) \quad (34)$$

To get values for iron, the known values for lead were used, since these values are more pronounced, particularly at the lower energies. In both Compton scattering and pair production, Eqs. (33) and (34) were applied over the entire range of energies.

Total attenuation coefficients,  $\mu$ , for all commonly used elements, including iron, are given in tabular form [16]. The mass absorption coefficients for tissue are also available in tabular form [21].

Finally, the data for the shielding materials and tissue were extended down to 0.01 MeV from 0.1 MeV, using values given in [6:173-4].

### 3. Full Data Tables

Table 2 gives the pair production data for all elements, which is zero for the first 17 discrete energy values used. Table 3 completes the data tables. Pertinent references are given below each table.

Table 2: Pair Production Attenuation Coefficients,  $\mu_{pp}$  ( $\text{cm}^2/\text{gm}$ )

Index Energy	Energy (MeV)	Water	Aluminum	Iron	Lead
17	1.0	0	0	0	0
18	1.25	0	0	0	0
19	1.5	0	0	.00067	.0018
20	2.0	0	.0007	.00160	.0043
21	3.0	.0012	.0018	.00392	.0105
22	4.0	.0019	.0032	.00634	.017
23	5.0	.0026	.0043	.00821	.022
24	6.0	.0032	.0053	.00932	.025
25	8.0	.0043	.0070	.01193	.032
26	10.0	.0051	.0087	.01417	.038

Reference: Water, aluminum, and lead data read from charts in [1:714-716]. Values for iron were obtained from those of lead.

Table 3: Attenuation Coefficients,  $\mu$  and  $\mu_c$  ( $\text{cm}^2/\text{gm}$ )

Index Energy	Energy (MeV)	Tissue	Water		Aluminum		Iron		Lead	
		$\mu_a$	$\mu$	$\mu_c$	$\mu$	$\mu_c$	$\mu$	$\mu_c$	$\mu$	$\mu_c$
1	.01	5.0	4.2	.214	22.0	.184	171.0	.118	80.0	.153
2	.015	2.0	1.4	.211	7.0	.180	56.6	.174	80.0	.149
3	.02	.70	.65	.204	3.2	.176	25.9	.170	80.0	.145
4	.03	.20	.33	.201	1.0	.174	8.36	.168	22.0	.142
5	.04	.095	.24	.193	.50	.172	3.74	.166	9.20	.139
6	.05	.055	.21	.190	.32	.163	2.00	.158	5.00	.136
7	.06	.037	.195	.187	.25	.160	1.19	.155	2.80	.133
8	.08	.028	.180	.170	.18	.153	.565	.148	1.25	.124
9	.10	.0271	.167	.163	.161	.145	.344	.140	5.29	.117
10	.15	.0282	.149	.147	.134	.134	.183	.129	1.84	.107
11	.20	.0293	.136	.140	.120	.118	.138	.114	.896	.097
12	.30	.0312	.118	.118	.103	.103	.106	.100	.356	.085
13	.40	.0317	.106	.106	.0992	.093	.0919	.090	.208	.076
14	.50	.0320	.0966	.097	.0840	.086	.0828	.083	.145	.070
15	.60	.0319	.0896	.090	.0777	.078	.0762	.075	.114	.063
16	.80	.0311	.0786	.078	.0683	.068	.0664	.066	.0836	.056
17	1.00	.0300	.0706	.071	.0614	.062	.0595	.060	.0634	.050
18	1.25	.0288	.0630	.064	.0548	.056	.0531	.054	.0596	.046
19	1.50	.0276	.0575	.057	.0500	.050	.0485	.048	.0512	.041
20	2.00	.0256	.0493	.049	.0432	.043	.0424	.042	.0457	.035
21	3.00	.0220	.0396	.039	.0353	.033	.0361	.033	.0421	.028
22	4.00	.0206	.0339	.032	.0310	.028	.0330	.027	.0420	.022
23	5.00	.0192	.0301	.028	.0282	.024	.0313	.023	.0426	.020
24	6.00	.0182	.0275	.025	.0264	.021	.0304	.020	.0436	.017
25	8.00	.0168	.0240	.020	.0241	.018	.0295	.017	.0459	.014
26	10.00	.0160	.0219	.017	.0229	.015	.0294	.014	.0489	.012

References: For tissue, [6], [16]; for  $\mu$  for all materials, [6], [16]; for  $\mu_c$  for all material except iron, [1:714-716]; and for iron,  $\mu_c$  was obtained from those of aluminum.



## APPENDIX C

## DETERMINATION OF THE POSITION OF EACH INTERACTION

In order to follow the progress of the particles through the materials of the shield to either their absorption or eventual emergence from the slab, a means must be devised whereby the coordinates of each event and the direction of each vector will be known in a fixed coordinate system. The fixed coordinate system used was such that the z-axis was perpendicular to the face of the shield and, in this study, coincided with the direction of the incident beam.

A second coordinate system used, called the local system, had as its origin the position of one interaction, as its z-axis, the local system had the direction defined by this origin and the position of the next interaction. The x and y axes were chosen on a plane perpendicular to the z-axis.

The direction cosines with respect to the local system, denoted by the primes, can be found from the standard geometric relationships between spherical and rectangular coordinates:

$$x_2' - x_1' = \Delta x' = r \cos\theta \sin\phi \quad (35a)$$

$$y_2' - y_1' = \Delta y' = r \sin\theta \sin\phi \quad (35b)$$

$$z_2' - z_1' = \Delta z' = r \cos\theta \quad (35c)$$

After dividing through by the distance, r, these become:

$$\Delta x'/r = \cos_x' = \cos\theta \sin\phi \quad (36a)$$

$$\Delta y'/r = \cos_y' = \sin\theta \sin\phi \quad (36b)$$

$$\Delta z'/r = \cos_z' = \cos\theta \quad (36c)$$

which are the direction cosines [20:539] of the emerging gamma vector relative to the local coordinate system. These are then transformed to direction cosines with respect to the fixed system to enable the location of successive interactions to be found (see Appendix D for the transformation used). The use of direction cosines simplifies tracking, especially when considering multi-region shields (see Appendix E) and in determining if an emerging particle will actually be detected.

Once these direction cosines in the fixed system are obtained, the point of the next interaction can be found in the fixed coordinate system. Using the next distance,  $r$ , selected, the position of the next interaction for the current gamma being tracked is:

$$x_2 = x_1 + r \cos_x \quad (37a)$$

$$y_2 = y_1 + r \cos_y \quad (37b)$$

$$z_2 = z_1 + r \cos_z \quad (37c)$$

where all coordinates and directions are in terms of the fixed system.

## APPENDIX D

## COORDINATE SYSTEM TRANSFORMATIONS

In each interaction from which a gamma-ray emerges, the angle of deflection,  $\theta$ , and the azimuthal angle,  $\phi$ , are measured from the previous gamma direction. A matrix transformation is required to rotate the local coordinate system, make it coincide with the fixed system, and produce the coordinates with respect to the fixed system. Then the location of the latest interaction can be found from the location of the previous event, which is already known in terms of the fixed system (see Appendix C).

The transformation matrix required is the product of two rotational matrices needed to align the local system with the fixed system. Figure 12a shows the first two vectors of a typical gamma history as viewed in the fixed system. The particle is started through the program at the plane  $z = 0$ , with some initial direction. After travelling a distance  $r_1$  to point #1, a Compton scattering occurs, sending the gamma toward point #2. Figs. 12b through 12c depict the sequence of coordinate transformations required to align the fixed system with the local system. The preliminary step (0) is to translate the origin of the fixed axes to the entry coordinates of point #0 (Fig. 12b). The superscripts (i) on each axis correspond to the number of the vector being considered. This vector is defined by  $(r_i, \theta_i, \phi_i)$ . The subscripts (j) denote the transformation step involved. The first rotation (step 1) is made through the angle  $\phi_j$  by fixing the  $z_0^1$ -axis (Fig. 12c). This aligns the new  $x_1^1$ -axis with

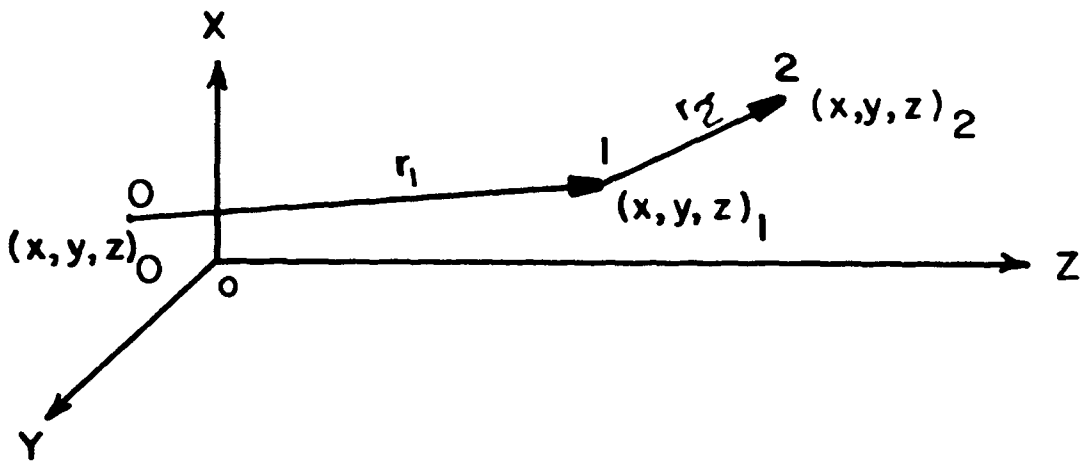


Figure 12a: Gamma tracking as seen from the fixed coordinate system.

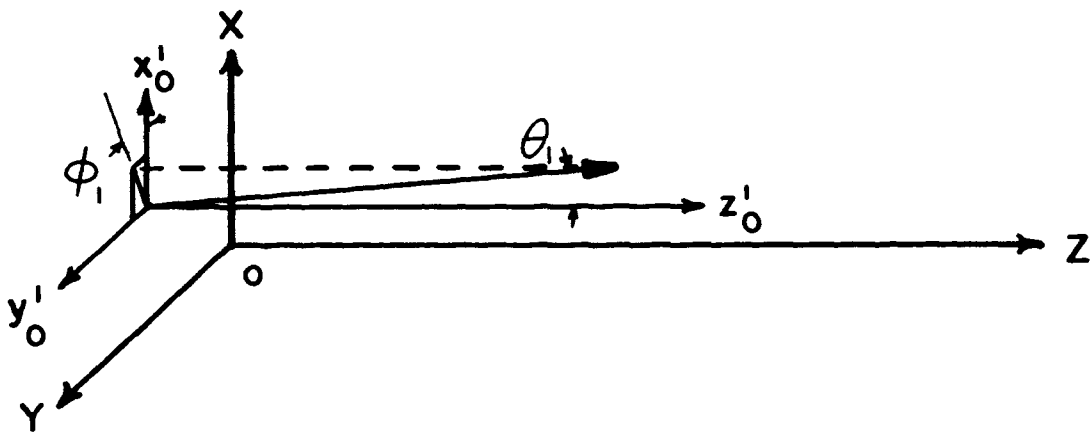


Figure 12b: Local System (Step 0) - Translate origin to the beginning of the first gamma vector.

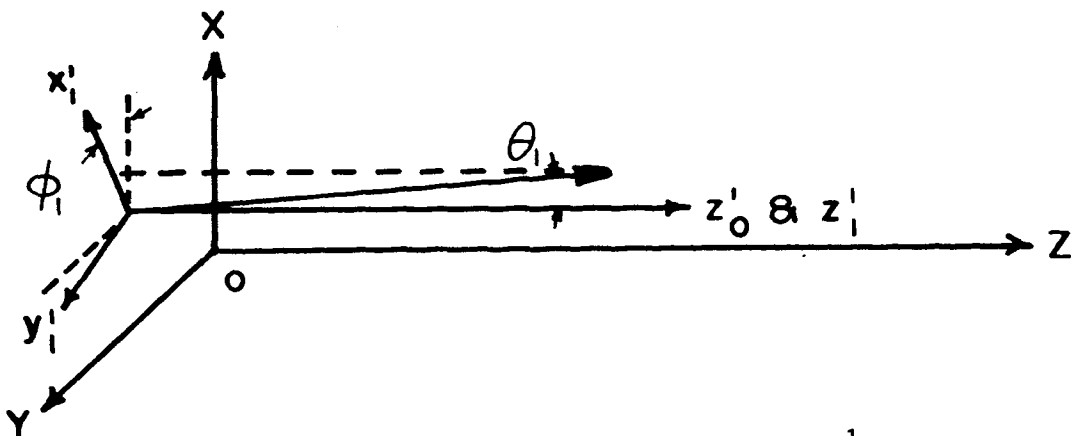


Figure 12c: Local System (Step 1) - Rotate about  $z_0^1$  through angle  $\phi_1$ .

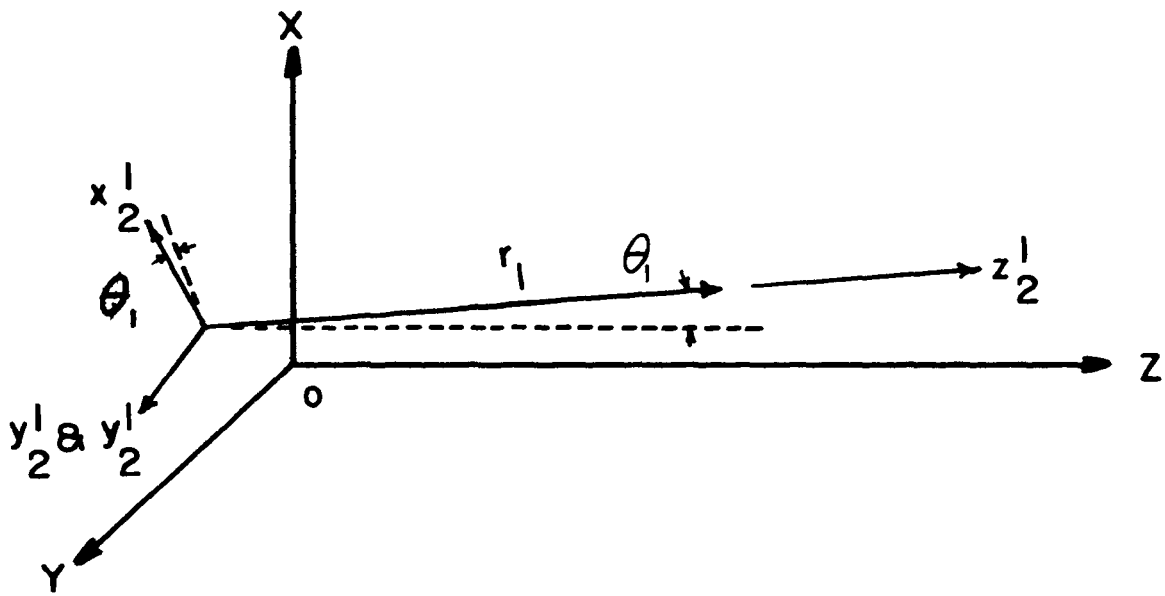


Figure 12d: Local System (Step 2) - Rotate about  $y_1^1$  through angle  $\theta_1$ .

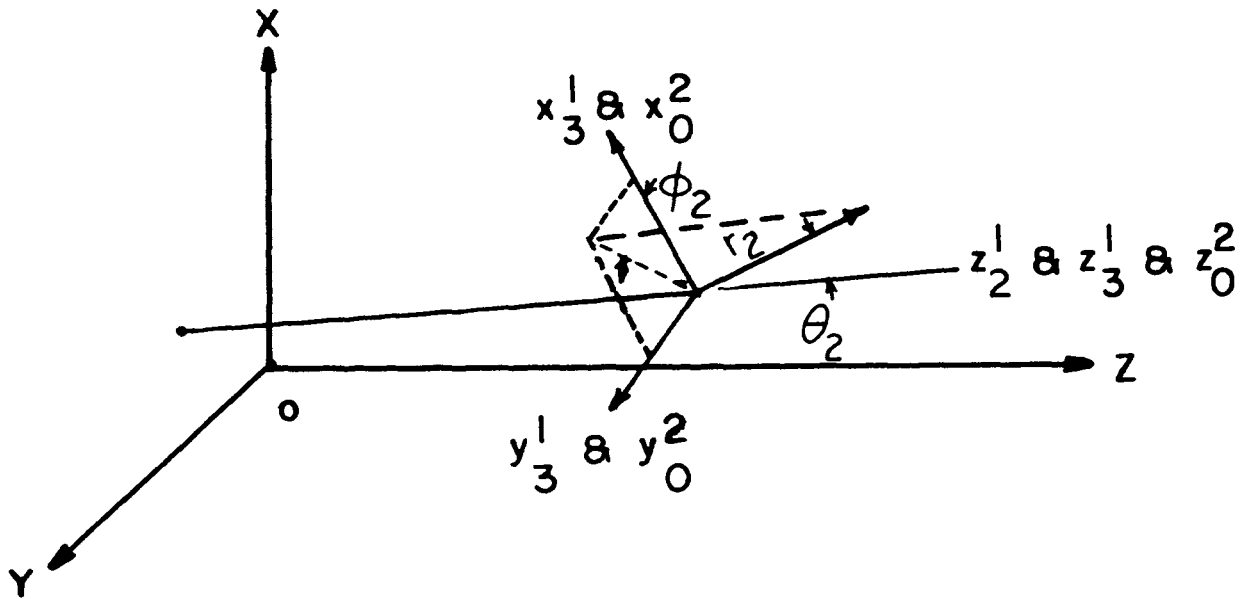


Figure 12e: Local System (Step 3) - Translate to the end of the current vector.

the first vector's projection on the fixed x-y plane. Next (step 2), a rotation is made through the angle  $\theta_1$ , holding the new  $y_1^1$ -axis stationary (Fig. 12d). This causes the latest local z-axis,  $z_2^1$ , to coincide with the current vector, as desired. Finally, the latest system is translated to the terminus of the first vector (Fig. 12e). The local system is now prepared for the second vector, defined by  $(r_2, \theta_2, \phi_2)$ . The new scattering angle,  $\theta_2$ , is measured from  $z_3^1 (=z_0^2)$ , the initial system for the second vector. The new azimuthal angle,  $\phi_2$ , is measured from the  $x_0^2$ -axis in the  $x_0^2$ - $y_0^2$  plane. Steps 1, 2, and 3 are repeated for each vector to force the local system after each interaction to coincide with the latest gamma vector.

These geometric transformations must be expressed mathematically to be used in the program. The translations are accomplished directly via Eqs. (35) of Appendix C. The rotations are accomplished using the product of the two transformation matrices corresponding to the separate rotations for  $\theta$  and  $\phi$  [21]. To perform step 1, rotate through the angle  $\phi_1$  by [22:25]:

$$\begin{bmatrix} x \\ y \\ z \end{bmatrix}_1^1 = \begin{bmatrix} \cos\phi_1 & -\sin\phi_1 & 0 \\ \sin\phi_1 & \cos\phi_1 & 0 \\ 0 & 0 & 1 \end{bmatrix} \begin{bmatrix} x \\ y \\ z \end{bmatrix}_0^1 \quad (38)$$

Next, step 2 requires rotation through  $\theta_1$ , leaving the latest y-axis unchanged; hence:

$$\begin{aligned}
\begin{bmatrix} x \\ y \\ z \end{bmatrix}_2^1 &= \begin{bmatrix} \cos\theta_1 & 0 & -\sin\theta_1 \\ 0 & 1 & 0 \\ \sin\theta_1 & 0 & \cos\theta_1 \end{bmatrix} \begin{bmatrix} x \\ y \\ z \end{bmatrix}_1^1 \\
&= \begin{bmatrix} \cos\theta_1 & 0 & -\sin\theta_1 \\ 0 & 1 & 0 \\ \sin\theta_1 & 0 & \cos\theta_1 \end{bmatrix} \begin{bmatrix} \cos\phi_1 & -\sin\phi_1 & 0 \\ \sin\phi_1 & \cos\phi_1 & 0 \\ 0 & 0 & 1 \end{bmatrix} \begin{bmatrix} x \\ y \\ z \end{bmatrix}_0^1
\end{aligned} \tag{39}$$

After performing the necessary matrix multiplication, Eq. (39) becomes:

$$\begin{bmatrix} x \\ y \\ z \end{bmatrix}_2^1 = C_1 \begin{bmatrix} x \\ y \\ z \end{bmatrix}_0^1 = \begin{bmatrix} \cos\theta_1 \cos\phi_1 & -\cos\theta_1 \sin\phi_1 & -\sin\theta_1 \\ \sin\phi_1 & \cos\phi_1 & 0 \\ \sin\theta_1 \cos\phi_1 & -\sin\theta_1 \sin\phi_1 & \cos\theta_1 \end{bmatrix} \begin{bmatrix} x \\ y \\ z \end{bmatrix}_0^1 \tag{40}$$

where  $C_1$  is the full transformation matrix required to convert point 0 from the local to the fixed system. The same can be done for the other end of the first vector, point 1. Hence:

$$\begin{bmatrix} x \\ y \\ z \end{bmatrix}_3^1 = C_1 \begin{bmatrix} x \\ y \\ z \end{bmatrix}_0^2 = \begin{bmatrix} \cos\theta_1 \cos\phi_1 & -\cos\theta_1 \sin\phi_1 & -\sin\theta_1 \\ \sin\phi_1 & \cos\phi_1 & 0 \\ \sin\theta_1 \cos\phi_1 & -\sin\theta_1 \sin\phi_1 & \cos\theta_1 \end{bmatrix} \begin{bmatrix} x \\ y \\ z \end{bmatrix}_0^2 \tag{41}$$

Eqs. (40) and (41) relate the end points of the first vector from the local to the fixed coordinate system. However, the main objective was to translate local direction cosines into direction cosines in the fixed system. Hence, subtraction of the coordinates for point 0 from point 1 yields:

$$\begin{bmatrix} x \\ y \\ z \end{bmatrix}_3^1 - \begin{bmatrix} x \\ y \\ z \end{bmatrix}_2^1 = C_1 \begin{bmatrix} x \\ y \\ z \end{bmatrix}_0^2 - C_1 \begin{bmatrix} x \\ y \\ z \end{bmatrix}_0^1 \Rightarrow \begin{bmatrix} x_3 - x_2 \\ y_3 - y_2 \\ z_3 - z_2 \end{bmatrix}^1 = C_1 \begin{bmatrix} x^2 - x^1 \\ y^2 - y^1 \\ z^2 - z^1 \end{bmatrix} \tag{42}$$

Upon expressing this as changes in each coordinate, dividing through by the length,  $r_1$ , of the vector in either system, and applying the translational relationship of Eqs. (35), we obtain:

$$\begin{bmatrix} x \\ y \\ z \end{bmatrix}_{\text{local}}^1 = C_1 \begin{bmatrix} x \\ y \\ z \end{bmatrix}_{\text{fixed}}^1 \Rightarrow \begin{bmatrix} \cos_x \\ \cos_y \\ \cos_z \end{bmatrix}_{\text{local}} = C_1 \begin{bmatrix} \cos_x \\ \cos_y \\ \cos_z \end{bmatrix}_{\text{fixed}} \quad (43)$$

Finally, since the local cosines are known directly from the local scattering angles for each interaction, invert Eq. (43) to obtain the direction cosines relative to the fixed system:

$$\begin{bmatrix} \cos_x \\ \cos_y \\ \cos_z \end{bmatrix}_{\text{fixed}} = (C_1)^{-1} \begin{bmatrix} \cos_x \\ \cos_y \\ \cos_z \end{bmatrix}_{\text{local}} \quad (44)$$

This completes the necessary coordinate transformation for the first vector's direction cosines. Note that since  $C_1$  is orthogonal, the inverse of  $C_1$  is merely its transpose  $C^T$  [22:25], and no inverse, per se, has to be calculated. To extend this to second and succeeding vectors, a new C matrix is developed for each interaction, and it is used to premultiply the product of previous transformation matrices. This is proper, since the product of a sequence of transformation matrices which are orthogonal is itself orthogonal [22:25]. Hence, using this product still results in a proper transformation. For the  $i^{\text{th}}$  vector we obtain:

$$\begin{bmatrix} \cos_x \\ \cos_y \\ \cos_z \end{bmatrix}_{\text{local}}^i = \prod_{n=1}^i C_n \begin{bmatrix} \cos_x \\ \cos_y \\ \cos_z \end{bmatrix}_{\text{fixed}}^i = C \begin{bmatrix} \cos_x \\ \cos_y \\ \cos_z \end{bmatrix}_{\text{fixed}}^i \quad (45)$$



Therefore, at each stage, the proper  $C_n$  matrix is used; but, to get fixed system direction cosines, the product matrix,  $C$ , is then inverted. Thus for the general case:

$$\begin{bmatrix} \cos_x \\ \cos_y \\ \cos_z \end{bmatrix}_{\text{fixed}}^i = (C)^{-1} \begin{bmatrix} \cos_x \\ \cos_y \\ \cos_z \end{bmatrix}_{\text{local}}^i \quad (46)$$

At the start of the program, the transformation matrix is initialized, based on the type of incident beam. In the case of normal incidence,  $\theta = 0$ . For a plane beam,  $\phi = 0$ , which means there originally is no  $y$ -component. Once these initial angles are determined (either constant for the entire run or selected differently for each particle), the initial direction cosines and the elements of the initial transformation matrix,  $C_0$ , can be calculated. If both a plane beam and normal incidence are selected, then the original directions are  $(0,0,1)$ , and the initial transformation matrix is the unit matrix.

## APPENDIX E

## TRACKING THROUGH MATERIAL INTERFACES

Once a method exists for obtaining the current vector orientation and its end point coordinates, all with respect to the fixed coordinate system, it is relatively easy to track the particle through the various interfaces between materials and determine when and where emerging particles leave the slab. Fig. 13 depicts the scheme which is used. The main technique is to use the law of cosines from analytic geometry which is, for a straight line:

$$\Delta x / \cos_x = \Delta y / \cos_y = \Delta z / \cos_z \quad (47)$$

The program will always have the current direction cosines available. Using the random distance selection scheme, the new coordinates are found. If these are not physically within the slab, there cannot be an interaction at this point; hence, they have no real meaning (see Pt. #7, Fig. 13). Using the coordinates of the previous event, which was within the shield (Pt. #5, Fig. 13),  $\Delta z$  is the difference between the known  $z$  value at the slab face and the previous  $z$ -coordinate.

Then, from Eq. (47) above:

$$\Delta x = \Delta z (\cos_x / \cos_z) \quad (48a)$$

$$\Delta y = \Delta z (\cos_y / \cos_z) \quad (48b)$$

These increments, when added to the previous coordinate values of  $x$  and  $y$ , respectively, yield the point of intersection (Pt. #6, Fig. 13) of the emerging vector with the particular  $z$  plane.

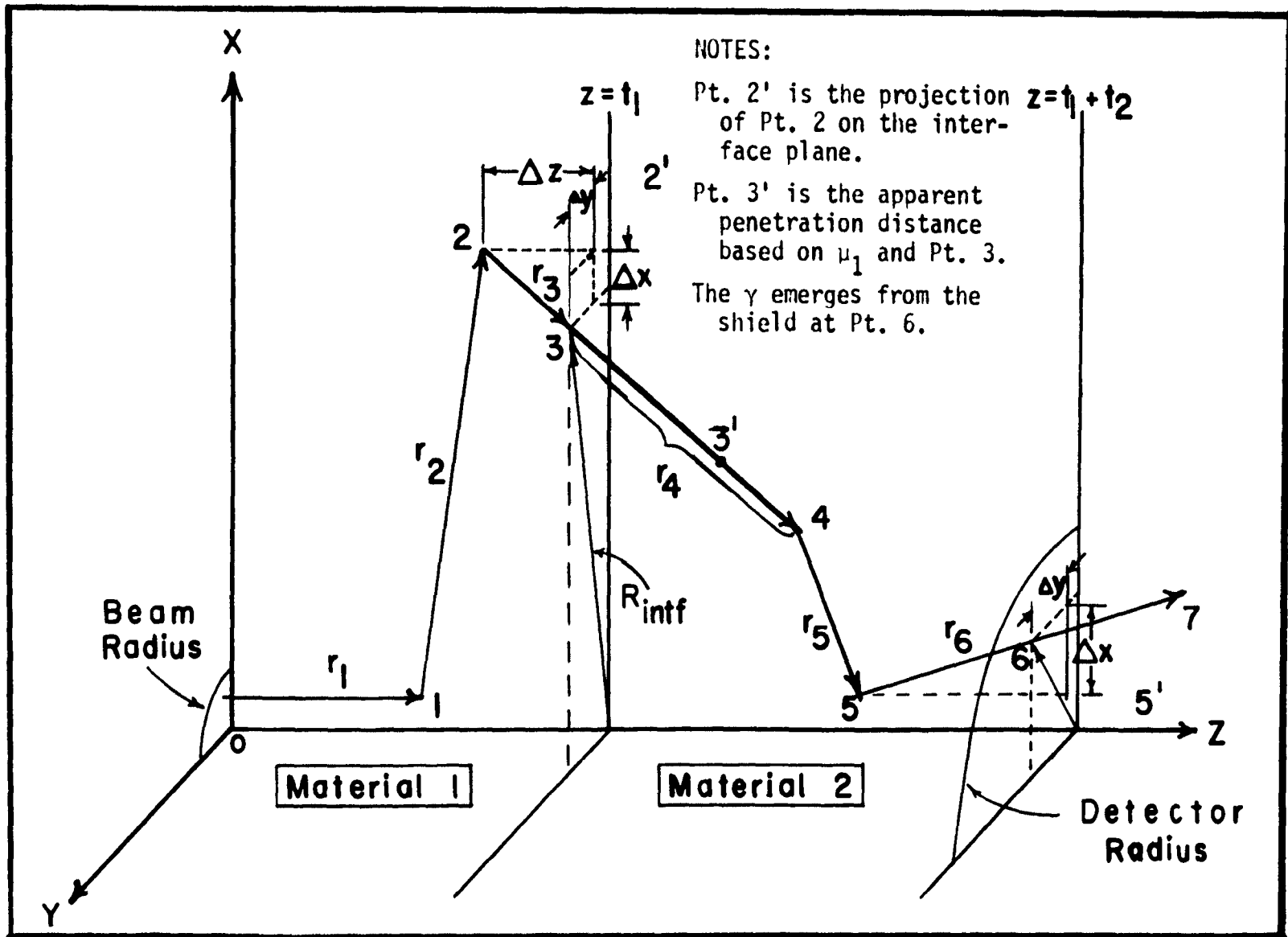


Figure 13: Gamma tracking through the interfaces of a double material shield.

This relationship is used primarily in the detection routine. However, it is also important to determine where a gamma vector intersects an interface between two shielding materials. Fig. 13 demonstrates this by showing passage from material region #1 to #2 along vector 2-3. The distance routine carries the gamma-ray to Pt. #3. However, since this new point is found to be in a new region, and the distance 2-3 was based entirely on the  $\mu_1(E)$  for the first material, the gamma actually reaches the interface at Pt. #3\* before a new distance calculation must be made. The program recycles to find a new value for  $\mu$ , based on the same energy,  $E_\gamma$ , but for material #2. Then an additional distance, based on  $\mu_2(E)$  is found, shown as vector 3\*-4, which is the correct penetration distance into the second material. Knowing the interface coordinates, this final increment can be applied to find the proper coordinates of the next interaction (Pt. #4, Fig. 13).

The main use of this routine is in the detection of emerging gammas. Both the beam and the detector are centered on the fixed z-axis. The detector is given a circular cross section by converting the specified area desired (input at the start of the program) into the radius the detector must have. Once a coordinate pair (x,y) is found for the gammas emerging from the last interface, the length of the radius vector from the z-axis to that point is determined. If that particular particle's radius vector upon emerging from the shield is greater than the detector radius, then the particle missed the detector. Otherwise, it has been detected.

## APPENDIX F

## ENERGY DEPOSITION ZONES

To describe how the electrons deposit their energy within the shield, a grid of zones was established inside the shielding material. This is solely for convenience in recording the energy deposition pattern. Such a system is shown in Fig. 14. This grid system is established prior to the run of each case to be considered. The actual thickness of each region is input in terms of mean free paths. This is immediately converted to centimeters for use in the main routine. The zone grid is then superimposed, using a preselected nominal grid size. Each material region is subdivided into equal sized zones, using the truncation property of fixed point variable and the relationship:

$$N_m = T_m/Z + \frac{1}{2} \quad (49)$$

where:  $N_m$  is the number of zones within the material region;  $T_m$  is the region thickness (cm); and  $Z$  is the nominal zone size desired (cm). For example, if  $Z$  is input as 1 cm,  $N_m$  will be truncated to 4 zones for thickness,  $T$ , between 3.50 and 4.49 cm. Then, the actual zone thickness to be used is:

$$\delta_m = T_m/N_m \quad (50)$$

This is done for each material region, and great care is taken to have the exterior zone boundaries coincide with the material region boundaries to simplify tracking. By establishing the zones in this manner, the energy deposited can be recorded efficiently, and the desired degree of resolution ( $\delta$ ) can be preselected for any run.

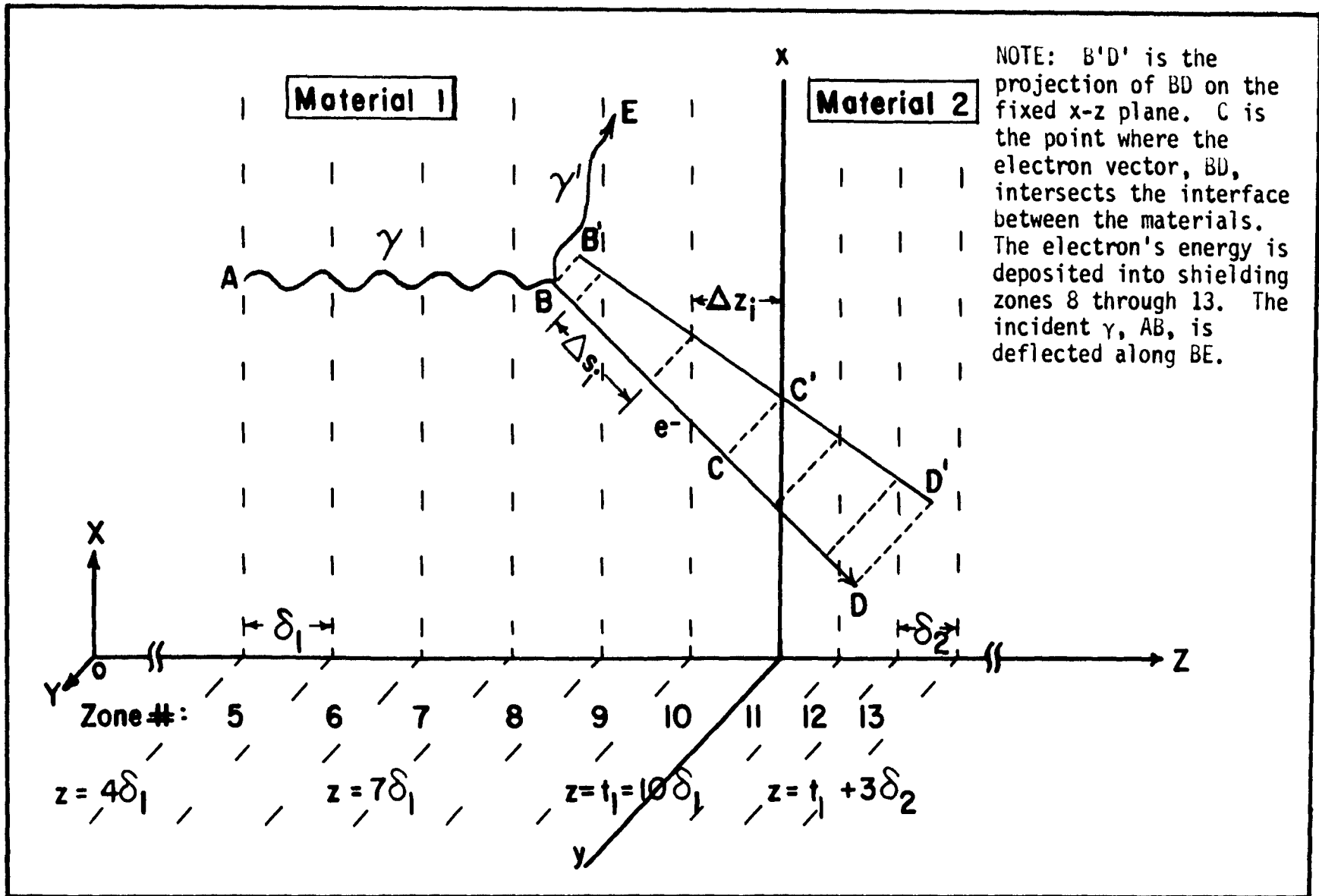


Figure 14: Electron tracking through the energy deposition zones of a double material shield.

To use Eq. (22) of section II.D.3.,  $\Delta S_i$  for each zone must be calculated for each electron path. From Fig. 14, the projection of the electron vector BD on the fixed x-z plane is given by B'D'. By similar triangles,  $\Delta z_i$  is proportional to the incremental path length in each zone. Hence:

$$\frac{\Delta S_i}{R} = \frac{\Delta z_i}{\Delta Z} ; \quad \text{or:} \quad \Delta S_i = R \frac{\Delta z_i}{\Delta Z} \quad (51)$$

where: R is the total length of the electron vector, and  $\Delta Z$  is the total z-component of that vector. From the basic definition of a direction cosine:

$$\cos_z = \Delta Z/R \quad (52)$$

Hence, we can use the known value of  $\cos_z$  for the electron to get:

$$\Delta S_i = \Delta z_i / \cos_z \quad (53)$$

The individual  $\Delta z_i$  are found when the affected zones are identified for the particular electron being considered.

## APPENDIX G

## ERROR ANALYSIS

To get a measure of the accuracy of the buildup factor calculations, the standard deviation and the relative error for each type of buildup factor was calculated. A general expression for the variance of a measurement is given by [5:18]:

$$\sigma^2 = \frac{N}{N-1} \left[ \frac{1}{N} \sum_{i=1}^R (\xi_i)^2 - (B^*)^2 \right] \quad (54)$$

where  $N$  is the total number of histories,  $R$  is the number of successes (defined in this case to be the number,  $N_c$ , of collided particles detected),  $\xi_i$  corresponds to the particular buildup factor, and:

$$B^* = \bar{\xi}_N = \frac{1}{N} \sum_{i=1}^R \xi_i \quad (55)$$

Hence, the variance can be rewritten as:

$$\sigma^2 = \frac{N}{N-1} \left[ \frac{1}{N} \sum_{i=1}^{N_c} \xi_i^2 - \left( \frac{1}{N} \sum_{i=1}^{N_c} \xi_i \right)^2 \right] \quad (56)$$

Then the standard deviation is merely  $\sigma$ , and the relative error (RE), expressed as a percent, becomes:

$$RE = 100(\sigma/B) \quad (57)$$

where  $B$  is the buildup factor under consideration. The error bars are then  $B \pm \sigma$ .

The various buildup factors, given in Eqs. (27), can be written in summation form as:



$$B_d = 1 + \frac{\sum_{i=1}^{N_c} \mu_i(E_i) E_i}{N \mu_0(E_0) E_0 e^{-\mu t}} \quad (58a)$$

$$B_e = 1 + \frac{\sum_{i=1}^{N_c} E_i}{N E_0 e^{-\mu t}} \quad (58b)$$

$$B_n = 1 + \frac{\sum_{i=1}^{N_c} (1)}{N e^{-\mu t}} \quad (58c)$$

The summation terms are the only "measured" quantities. The other factors are defined by the run parameters. Hence, we can rewrite each of Eqs. (58) as:

$$B_d^* = (B_d - 1) \mu_0(E_0) E_0 e^{-\mu t} = \frac{1}{N} \sum_{i=1}^{N_c} \mu_i(E_i) E_i \quad (59a)$$

$$B_e^* = (B_e - 1) E_0 e^{-\mu t} = \frac{1}{N} \sum_{i=1}^{N_c} E_i \quad (59b)$$

$$B_n^* = (B_n - 1) e^{-\mu t} = \frac{1}{N} \sum_{i=1}^{N_c} (1) = \frac{N_c}{N} \quad (59c)$$

Eqs. (59) are in the form of Eq. (55). Hence:

$$(\xi_i)_d = \mu_i(E_i) E_i \quad (60a)$$

$$(\xi_i)_e = E_i \quad (60b)$$

$$(\xi_i)_n = 1 \quad (60c)$$

Now Eqs. (56) and (59) can be applied to get the variance for each buildup factor:

$$\sigma_d^2 = \frac{N}{N-1} \left[ \frac{1}{N} \sum_{i=1}^{N_c} (\mu_i E_i)^2 - (B_d^*)^2 \right] = \frac{1}{N-1} \sum_{i=1}^{N_c} (\mu_i E_i)^2 - \frac{N}{N-1} (B_d^*)^2 \quad (61a)$$

$$\sigma_e^2 = \frac{N}{N-1} \left[ \frac{1}{N} \sum_{i=1}^{N_c} (E_i)^2 - (B_e^*)^2 \right] = \frac{1}{N-1} \sum_{i=1}^{N_c} E_i^2 - \frac{N}{N-1} (B_e^*)^2 \quad (61b)$$

$$\sigma_n^2 = \frac{N}{N-1} \left[ \frac{1}{N} \sum_{i=1}^{N_c} (1)^2 - (B_n^*)^2 \right] = \frac{1}{N-1} (N_c) - \frac{N}{N-1} (B_n^*)^2 \quad (61c)$$

Finally, for a sufficiently large number of histories, we can simplify Eqs. (61) by using  $(N-1) \doteq N$ . Hence:

$$\sigma_d^2 \doteq \frac{1}{N} \sum_{i=1}^{N_c} (\mu_i E_i)^2 - (B_n^*)^2 \quad (62a)$$

$$\sigma_e^2 \doteq \frac{1}{N} \sum_{i=1}^{N_c} E_i^2 - (B_e^*)^2 \quad (62b)$$

$$\sigma_n^2 \doteq \frac{N_c}{N} - \left( \frac{N_c}{N} \right)^2 = \frac{N_c}{N} \left( 1 - \frac{N_c}{N} \right) \quad (62c)$$

Eqs. (57) give the variance of the starred quantities (Eq. (55)). To get the standard deviation of the unstarred quantities (Eqs. (58)), use is made of the fact that:

$$\sigma_B = \frac{\sigma_{B^*}}{\mu_0 E_0 e^{-\mu t}} \quad (63)$$